

THE DESIGN, CONSTRUCTION AND TEST RESULTS OF A SMALL CENTRIFUGE  
AEROSOL SPECTROMETER FOR FINE PARTICULATE

Paul L. Anderson  
Principal Investigator  
Kaiser Aluminum & Chemical Corp.  
Center For Technology  
Pleasanton, CA. 94566  
October 1973

Final and summary report to California Air  
Resources Board covered by Agreement ARB 2-290.

LIBRARY  
AIR RESOURCES BOARD  
P. O. BOX 2815  
SACRAMENTO, CA 95812

## Report-In-Brief

A centrifuge ambient aerosol sampling device for very small particles has been designed, built and tested. The unit is compact, hand carriable, and built into a suitcase sized enclosure. The sampling head consists of a spirally shaped processor annulus machined into an aluminum cylinder about 3-1/4" in diameter. A centrifugal force precleaner provides a clean process carrier gas through which the particles of the sample aerosol are spectrally separated. The sized particles may be deposited on to any thin substrate such as mylar, paper or metal foil. The deposited particles occur as a spectral distribution of sizes along the length of the collector strip. One calibration ranges from 0.16 to 1.6  $\mu\text{m}$ ; a second tentative calibration ranges from 0.9 to 8  $\mu\text{m}$ . A 5% calibration precision was attained. The analytical sampling rate is 1 ml/sec. The collected particulate is remarkably amenable to scanning electron microscopic analysis. Attempts to do direct chemical analyses on the particulate by an energy dispersive x-ray method has been unsuccessful, probably because of insufficient sensitivity of the x-ray instrument.

## TABLE OF CONTENTS

	Page
1.0 INTRODUCTION-----	1
2.0 THEORY AND APPLICATION-----	5
3.0 DESIGN AND CONSTRUCTION DETAILS-----	11
3.1 Centrifuge parts-----	11
3.2 Collector Strips and Their Containers-----	13
3.3 Motor and Speed Controller Descriptions-----	15
3.4 Sampler Head Assembly-----	16
3.5 Components Case-----	16
3.6 Assembly, Balancing and Speed Control Test-----	17
4.0 SPLIT RATIO DETERMINATION-----	27
5.0 CALIBRATION-----	31
6.0 ENTRY LOSS DETERMINATION -----	43
7.0 SAMPLING AND RESULTS-----	51
7.1 Preliminary Field Tests-----	51
7.2 Samples from Pomona, California-----	52
APPENDIX A BLUE PRINTS AND SPECIFICATION SHEETS-----	A-1
APPENDIX B AEROSOL GENERATOR DESCRIPTION-----	B-1
APPENDIX C CHARACTERIZATION OF SYNTHETIC AEROSOL-----	C-1
APPENDIX D LIST OF SPECIFIC SUPPLIERS-----	D-1

## 1.0 Introduction

In a nonturbulent fluid the settling velocity of small particles is predictable by the Cunningham corrected Stokes law:

$$v_s = \frac{d^2 g}{18\mu} (\rho_p - \rho) C \quad (\text{Eg. 1})$$

where  $d$  = particle diameter

$\mu$  = viscosity of the fluid medium

$\rho$  = density of the fluid medium

$\rho_p$  = density of the particle

$g$  = acceleration by gravity

$$C = 1 + \frac{2\lambda}{d} [1.257 + 0.4 \exp(1.1 \frac{d}{2\lambda})]$$

$\lambda$  = mean free path of gas molecules

Solution of the stokes equation for several different sized particles yields the following sedimentation velocities:

Particle Diameter ( $\mu\text{m}$ )	Sedimentation Velocity	
	cm/sec	cm/day
100.0	24.8	$2.1 \times 10^6$
10.0	$3.1 \times 10^{-1}$	$2.7 \times 10^4$
1.0	$3.5 \times 10^{-3}$	$3.0 \times 10^2$
0.1	$8.6 \times 10^{-5}$	$7.4 \times 10^{-1}$

Considering normal atmospheric turbulence, the precipitation velocity for submicron particles is virtually zero, i.e., they stay suspended. Only with natural growth by interception and agglomeration do they become large enough to precipitate. The submicron particles, because their size approximately matches the wavelength of visible light, disproportionately scatters light and gives rise to a dirty look to the air over metropolitan

areas. Also, because of their small size, the submicron particles are especially difficult to collect and study.

The principal of inertial force to size classify and collect fine particles is used in three basic types of sampling instruments: 1) inertial impactor, 2) centrifuge, and 3) cyclone. The later type is the simplest but also the least precise and not applicable to submicron particles. Inertial impactors are mechanically simpler than centrifuges but better resolution and application to smaller particles is achieved with centrifuges (Ref. 3).

Irrespective of design detail the mechanism of centrifuge type aerosol spectrometers is to increase the particle's effective mass by centrifugal force, drive the particles across a moving clean air stream for size separation, and collect the sized particles on the outer wall of the curved air channel (annulus).

In all the centrifuge aerosol spectrometer designs preceeding Hochrainer's (Ref. 1), the clean process air supply was from an independent source. In Hochrainer's device the centrifuge itself generates its own carrier gas supply by cleaning a portion of the sampled aerosol in a precleaning annulus; also, the device was unique in that it acted as its own sampling pump and was very small and portable. Those features resulted in a small and mechanically simple device capable of sampling and spectrometrically processing submicron particles with unusually high resolution.

Hochrainer's design was tested at Kaiser Aluminum Corporation's Center for Technology (CFT) where Hochrainer's

results were confirmed (Ref. 4). The sampler's characteristics and analytical results indicated it to be particularly applicable to ambient aerosol sampling of submicron particles. Conversations with people of the Research Branch of California Air Resources Board suggested they would entertain a proposal for a feasibility study of a small centrifuge sampler. The attractive features of the envisioned device for ARB application included, 1) the ability to spectrally collect particles as individuals for subsequent scanning electron microscopic examination and description and 2) the potential for this sampler's use to collect spectrally distributed particulate for chemical analysis by the University of California (Davis) cyclotron x-ray analytical system. The proposal (Ref. 5) titled "A Feasibility Study of a Field Model, High Resolution Centrifuge Spectrometer to Determine Particle Size Distribution in the range of 1.5 to 0.15  $\mu\text{m}$  and Provide Samples for Direct Electron Microscope Characterization" was submitted in August, 1972 and was formally accepted by ARB in September, 1972.

Certain requirements and proposed improvements demanded design specifications different from Hochrainer's. The height of the process annulus was doubled, to two centimeters, to provide a collector strip width sufficient for the x-ray analytical system. The process annulus was to be in the form of a spiral, rather than a circle, in order to provide a full order-of-magnitude of sizing range. An entirely different precleaner design would lessen spectral contamination by particles that

penetrate the precleaner. The sampler must be compact, portable and capable of prolonged unattended operation.

## 2.0 Theory and Application

The theory of particle deposition in the annulus of a centrifuge is most easily envisioned in a circular annulus as in the Hochrainer device. Figure 1 shows a descriptive diagram of the equipment and the analytical process in the Hochrainer centrifuge. Particle deposition is based on the assumption of laminar carrier (process) gas flow in the annulus. Radial particle velocity  $v_r$  is a function of centrifugal force. Hochrainer (Ref. 1) developed his modeling equation as follows:

$$v_r = \frac{2\pi^2}{9\eta} D^2 \rho R V^2 C \quad (\text{Eq. 2})$$

$\eta$  = viscosity of carrier gas

$D$  = particle spherical diameter

$\rho$  = particle density

$V$  = rotational speed of the particle  
(rotor plus linear velocity of carrier gas)

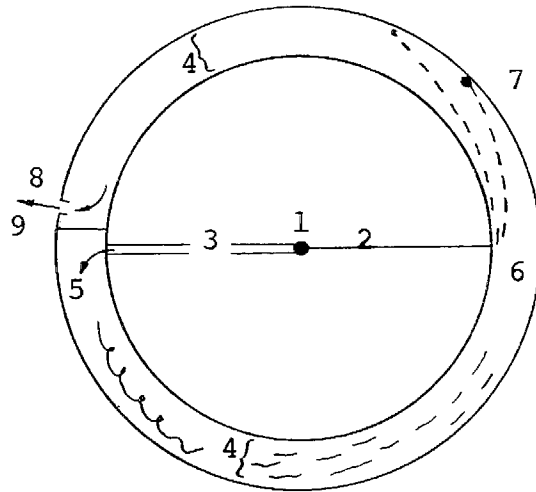
$R$  = radius; the distance of the particle from  
the center of rotation

$C$  = Cunningham slip correction factor  
(Same as in equation 1)

Particle trajectory from the inner radius  $R_1$  to the outer radius  $R_2$  of the annulus can be integrated to give  $Z$ , the projection to the outer wall of the annulus:

$$Z = \frac{9\eta F}{2\pi^2 R_1 D^2 \rho V^2 C} \quad (\text{Eq. 3})$$

$Z$  = position (distance from zero) on the collector strip



1. Aerosol entry (from top).
2. Narrow aerosol channel for analytical stream.
3. Wide aerosol channel for carrier gas.
4. Annulus.
5. Turbulent aerosol.
6. Cleaned, laminar carrier gas.
7. Particles being sized and spectrally deposited.
8. Exit orifice.
9. Membrane.

Figure 1

Diagram of the operational mechanism of a circular annulus aerosol spectrometer. Aerosol enters at 1, splits into streams 2 and 3, and is lead to annulus 4. Stream 5 is cleaned and made laminar (6) to spectrally process aerosol 7. All the sampled air leaves through the orifice 8 just ahead of membrane 9.

This trajectory in a spirally shaped annulus would conform to equation 3,  $R_1$  being a continuous variable as the radius of the annulus expands.

Figure 2 is a sketch of the spiral annulus concept. In this version the precleaner, positioned above the plane of the diagram and not shown here, feeds cleaned air to the laminating section which begins at point A. The stream makes about  $360^\circ$  of travel in the first wrap of the annulus. It has become laminar at point F where the analytical aerosol enters. Coarser particles rapidly migrate across the process stream (G) because of their greater mass; smaller particles (H and I) have a lower trajectory angle and collect farther down on the outer annulus wall. The spiral annulus thus provides nearly  $360^\circ$  of laminating zone and an additional  $360^\circ$  of spectral zone, rather than about  $180^\circ$  each as in a circular annulus. A suitable thin collector strip positioned on the outer wall facilitates removal of the collected particles for subsequent analyses.

The precleaner section for the present centrifuge consists of a narrow circular annulus in a separate body positioned directly above the laminating and analytical section. In the precleaner as diagramed in Figure 3 the aerosol enters at (1), follows a two millimeter wide channel (2) to a 3 millimeter wide circular annulus (3); the aerosol is thus immediately brought to a maximum centrifugal force on the extreme of the precleaner's radius. The aerosol is cleaned by centrifugal force through  $345^\circ$  of this annulus and then follows a second two millimeter wide channel (4) back to a point near its origin. A hole



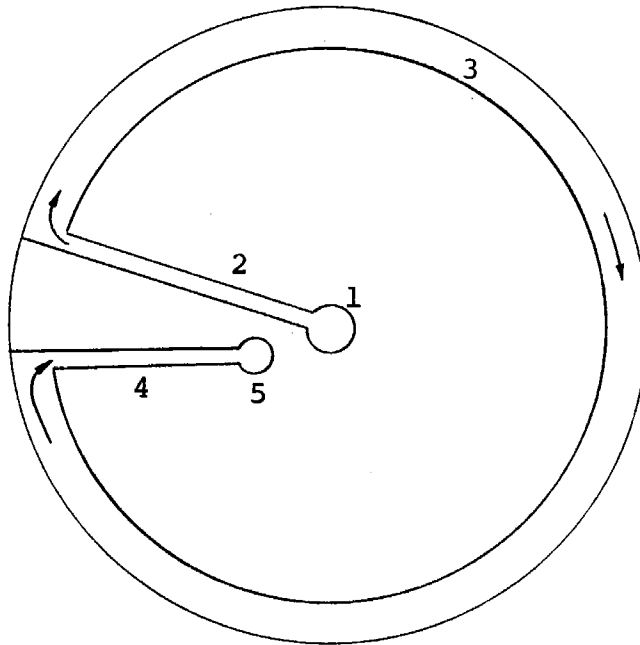


Figure 3

Diagram of the precleaner section. The aerosol enters the top of the sampler through the central hole (1), follows the channel (2) out to the circular annulus (3), makes nearly a full revolution for cleaning and is then brought back to near the point of origin by a second channel (4). The cleaned air then drops down to the beginning of the laminating spiral (A in Figure 2).

in the bottom of the precleaner (5) is positioned directly over the beginning of the spiral laminator section (point A) in Figure 2.

Equation 3 was used to calculate the maximum particle size which could escape the cleaning annulus and was found to be  $0.066 \mu\text{m}$  at the expected centrifuge speed. This is about one-half the size of the smallest particle in the spectral distribution. The precleaner in Hochrainer's centrifuge removed particles from the carrier gas only as small as the smallest particle in the spectral distribution. This was a source of considerable contamination.

Repeated computerized solutions to equation 3 prescribed the final dimensions and expected operating parameters for the spiral annulus analytical section. The results were

Annulus height,	20 mm
Annulus width,	5 mm
$R_1$ (Beginning of spiral)	15 mm
$R_1$ (End of spiral)	29 mm
Annulus wall thickness	2 mm
Z (Collector wall length)	192 mm
V (Rotational speed)	10,000 RPM
F (Flow rate)	11.2 ml/sec.
Maximum particle size (at 3mm)	$1.5 \mu\text{m}$
Minimum particle size (at 170mm)	$0.12 \mu\text{m}$

### 3.0 Design and Construction Details

#### 3.1 Centrifuge Parts

With dimension specifications and consultation, the engineering design branch at CFT developed design detail and subsequently blue prints for the sampler. Copies of these prints are included in Appendix A of this report. Four separate sampling units were then built.

The following is a description of the individual components shown on the blue prints. The bottom of the sampler body includes a standard #1 tapered hole to receive the motor shaft. The sampler body is secured to the motor shaft by a groove-snap ring-nut assembly. The precleaner section is mounted directly on top of the analytical section and is positioned by locating dowels. A hollow cap fits over and around the precleaner section and secures the precleaner to the sampler body by screwing on to the body section. The inside wall of the hollow cap serves as the collector wall for the precleaner section.

A fault in the original design was detected early in the sampling program. It was found that aerosol was leaking past the web which separates the two channels in the precleaner section. This allowed raw aerosol to leak into the laminator section without first being cleaned. This problem was corrected by machining a narrow verticle slot in the metal web and fitting the slot with a teflon bar. In operation centrifugal force moves the teflon bar out against the wall of the cap forming a seal.

The tube which conducts the analytical sample past the precleaner into the sampler body is secured by a press fit into the center of the precleaner section. The tube extends, by close fit, into the sampler body to release the analytical aerosol to the collimating insert midway in height of the spiral annulus. This provides for good particulate distribution over the height of the analytical annulus, a noticeable deficiency in Hochrainer's centrifuge.

The aerosol of the analytical sample enters the clean, laminar carrier gas through a narrow slot machined into the collimating insert. The slot functions both to collimate and to regulate the amount of analytical aerosol admitted to the carrier gas. The collimating slot is in the form of a shallow gain in one side of an aluminum plug. The plug forms an insert which fits in a recess between the center of the sampler body and the inside wall of the spiral analytical annulus. The depth of the collimating slot is critical and was defined experimentally as described in a later section of this report.

The final exit hole for the combined carrier gas and processed analytical air is at the end of the spiral annulus. This hole was drilled, tapped and fitted with a 1/4" threaded plug. An exit orifice was later drilled into the plug. The size of this orifice limits the flow rate, a factor affecting calibration range, and is therefore critical. Its size was also experimentally determined as is later described.

Bids for construction of the centrifuge components were

received from two shops. The bid submitted by Beimer's Machine Works, Inc.\* was accepted.

After fabrication the 6061-T6 aluminum alloy of the sampler parts was anodized at CFT with 0.8 mil of Kalcolor. The anodized surface prevents the screw threads from binding and protects the sampler's surface.

### 3.2 Collector Strips and Their Containers

Part of the justification for this work was to investigate the feasibility of this sampler to collect sized particulate for analysis by the cyclotron-x-ray analytical method at the University of California, Davis. One requirement for this analytical system is to have a substrate of minimum mass which is "x-ray transparent". The research personnel at Davis examined and accepted 6  $\mu$ m thick mylar plastic which is used at CFT for certain x-ray analyses. Virtually any thin material - plastic, paper, metal foil - can be used as collector substrate so far as the sampler is concerned. This mylar is acceptable for purposes of the sampler except it lacks sufficient body to be self supporting. Also, any contamination the mylar picked up on its back, against the annulus wall, would confuse the analytical result. These problems were solved by designing a double layer collector strip of mylar substrate supported on thoroughly cleaned aluminum foil. The foil is 0.08 mm thick, full-hard tempered 1199 alloy.

---

\*A list of specific suppliers is found in Appendix D.

Double coated cellophane tape was used at the ends of the mylar to attach it to the foil. The foil is 30 cm long, the mylar 23 cm long. With these lengths the mylar extends from the outlet of the sampler to about 5 cm upstream of the entry point of the analytical sample (into the laminating zone). The foil extends 7 cm further into the laminating annulus, but does not cover the entire outer wall of the double spiral. The stiffness of the foil holds it against the outer wall of the annulus. The mylar is supported in proper position by the foil.

To construct the collector strips, double coated cellophane tape was attached to the foil at the required locations. The 4" wide mylar is dispensed from a 9" diameter spool. In construction the foil was wrapped tightly around the mylar spool's curved surface. The tape adhered to the mylar at the required points. Wrapping the foil around the mylar spool conveniently provided the slightly shorter length requirement for the mylar, compared to the foil, that results from the inside curvature of the sampler annulus. These 4" wide double layers were then sliced lengthwise by a wheel type paper-foil cutter into 19 mm widths to fit the height of the annulus. This entire procedure was done inside a clean box.

Containers for the collector strips were fabricated from 1" O.D. glass tubing (App. D). The tubing was cut into 13" lengths with a diamond blade saw. They were then thoroughly cleaned and air dried in a clean box. The prepared collector strips were inserted into the glass tubes and the ends stoppered

with cleaned #4 rubber stoppers; again, all in the clean box. These glass containers provide convenient protective containers for the collector strips both before and after exposure. Sample identification can be written directly on the container with a "felt pen".

### 3.3 Motor and Speed Controller Descriptions

The selection of the motor and drive-speed controller followed a frustrating search in the world of fractional horse-power motors and controllers. It is believed at this point that the motor and controller combination selected was, though fortuitous, particularly good. Both units have performed well during about 500 hours of operation. Life expectancy of the brushes in the D.C. motor is 800 to 1000 hours.

The motor is a Globe D.C. permanent magnet, type GRP, 1/12 HP. Detailed specification appear in Appendix A. The motor measures 2-1/4" in diameter and 3-3/4" long (minus shaft). For this application the motor shafts were replaced by a longer tapered and grooved shaft for connection to the centrifuge body.

The motor is powered and its speed is selected and controlled by a magnetic pick-up feed-back system. This unit was supplied by Detection Sciences, Inc. and is described in detail in Appendix A. In this system a magnetic sensor is mounted on the front face of the motor near a 20 tooth sprocket mounted on the motor's shaft. By magnetic sensing the controller counts sprocket teeth for two seconds, converts the count to RPM and compares that to the set speed. It then corrects by adding or

subtracting voltage to the motor. The speed selector is digital on "thumb wheels" with each minimum digit registering 100 RPM. The maximum speed is preset at 15,000 RPM. The controller repeatedly integrates magnetic signals for two seconds, compares, corrects and makes a lighted display of the actual speed for the previous time interval.

This provides an internal visual check. Such a system eliminates the need for calibrations and provides for precision in speed selection. The speed is only temporarily affected by voltage fluctuations. Specification sheets on these components are found in Appendix A.

#### 3.4 Sampler Head Assembly

The centrifuge is mounted on to the motor's shaft. The motor is clamped in a circular cut-out in a 6" x 6" x 3/8" thick aluminum plate. The plate is attached to a 3/4" diameter aluminum conduit pipe as a support post. A safety cage made from perforated aluminum sheet encloses the sampler head and attaches to the square support plate. It protects the centrifuge from large objects and also serves as a safety shield in case the centrifuge should come loose from the motor.

#### 3.5 Components Case

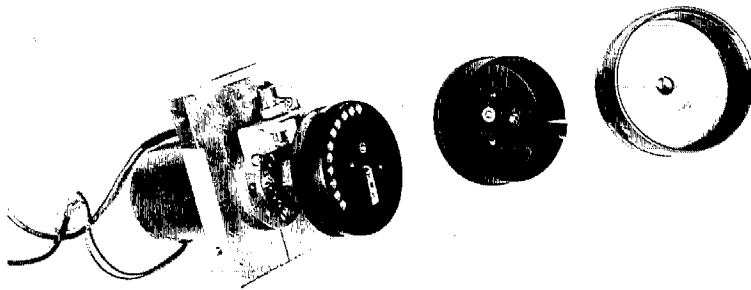
The electric power and speed controller components were mounted inside a standard 20" x 16" x 7-1/2" electrical switch

box. A cut-out was made on the front of the box to receive the face plate of the speed selector-controller. Removable legs attach to the bottom of the box when sampling, and pack inside when transporting. The sampler support post, with sampler head, attaches to the side of the box during sampling and packs inside the box for transporting. A removable steel cover fits over and protects the face plate during transporting. The result is that the entire sampler assembly is portable in one carrying case which conveniently unfolds to sampling arrangement with only the addition of 110 V electrical power.

### 3.6 Assembly, Balancing and Speed Control Tests

The components were assembled and tested at slow speed for continuity and then they were dynamically balanced.

Figure 4 is a photograph of a disassembled sampler head. Points of interest in the photo are 1) the motor clamped in the mounting bracket, 2) the magnetic pick-up and sprocket, 3) the sampler body with the spiral annulus, 4) the collimating insert (bright aluminum), 5) holes drilled in the rim of the body for balancing, 6) the precleaner section which fits superimposed on the sampler body, 7) the two channels for a) leading the aerosol to the precleaner annulus and b) for leading the cleaned air back to be fed down into the beginning of the laminating annulus, 8) the centrally located analytical tube in the precleaner section, 9) the cap which fits over the precleaner and secures it by screwing onto the body, 10) the inside wall of the cap is the collector wall for the precleaner annulus.

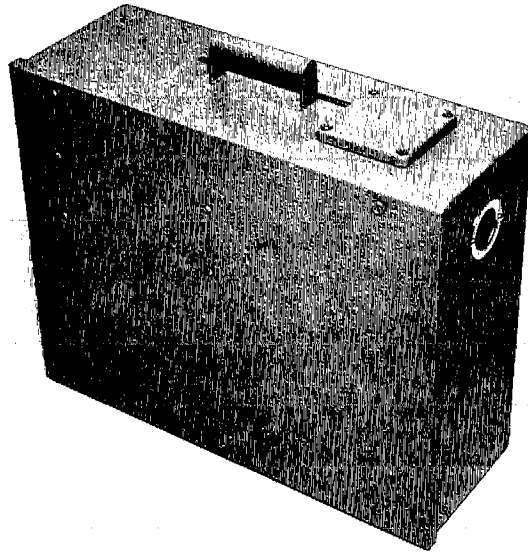


H26084

Figure 4  
VIEW OF A DISASSEMBLED SAMPLER HEAD

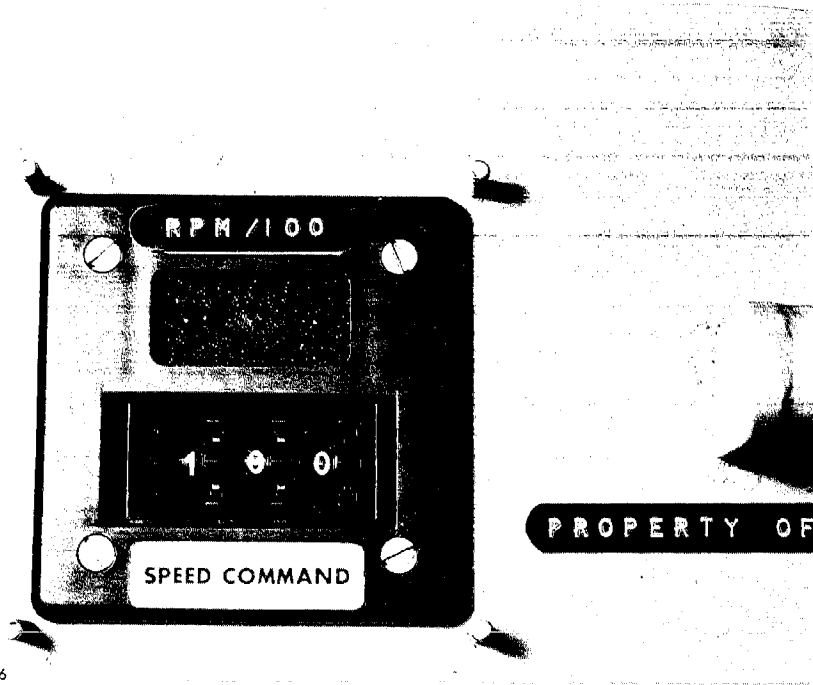
Figure 5 shows a view of the sampler packed for transporting. The small square cover to the right of the handle protects the speed controller's face plate. A close up of the face plate is shown in Figure 6. The three thumb wheels are used to select the speed in 100 RPM intervals; the window above the selectors show by lighted numbers the actual speed. Figure 7 shows the sampler with its lid open exposing the controller electronics, the sampler head with its safety cage, and the legs in their rack on the inside of the lid. Figure 8 is a view of the assembled sampler ready for sampling. Figure 9 shows an aluminum-mylar collector strip inside its glass container.

A test was made to determine the effectiveness of the speed selector and controller. Though an available strobe light tachometer was capable of determining the speed, its stated precision was only 1% of the set value, a value which is the upper limit of the speed variation specified for the controller. For a more precise test a special triggering and monitoring circuit that would drive the strobe was devised. This circuit consisted of a variable frequency generator to directly trigger the strobe tachometer. A "T" from this circuit to a frequency counter made it possible to count exactly the triggering frequency, i.e. RPM. A diagram of this test arrangement is shown in Figure 10. The stability of the frequency counter was tested and found to be better than 0.01% in 15 minutes, a very favorable value compared to the possible 1% variation being tested. Both short and longer time tests were



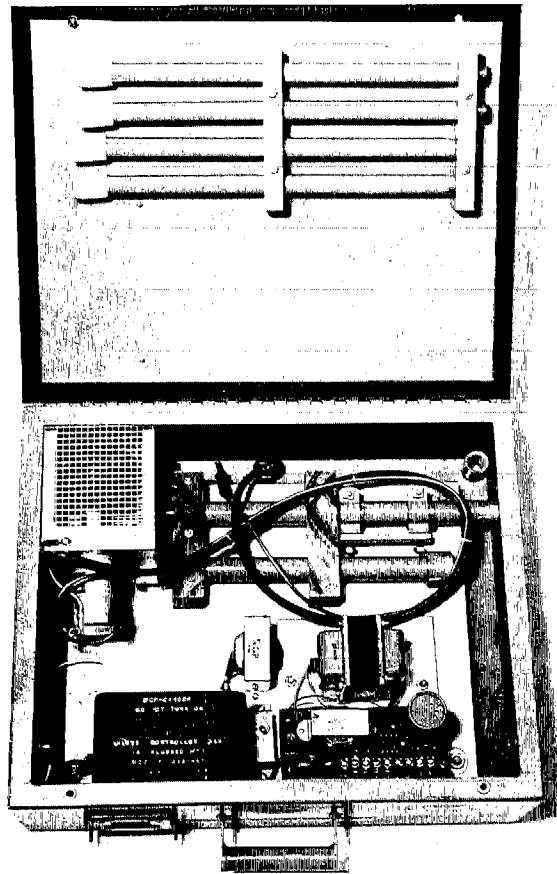
H26085

Figure 5  
VIEW OF THE SAMPLER PACKED FOR TRANSPORTING



H26086

Figure 6  
VIEW OF THE SPEED CONTROLLER FACE PLATE



H26087

Figure 7  
VIEW OF THE SAMPLER WITH THE LID OPEN EXPOSING  
THE INSIDE COMPONENTS AND PACKED SAMPLER

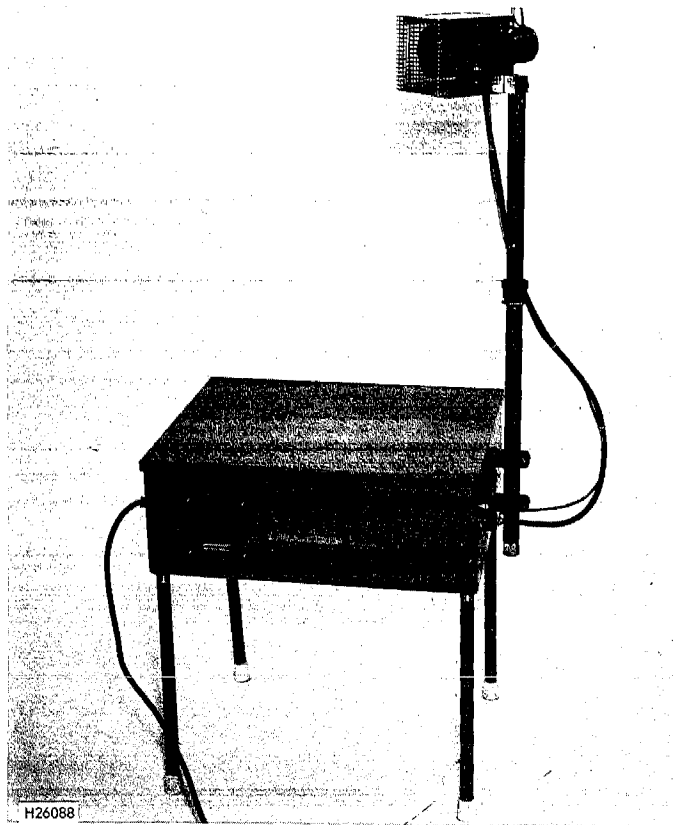
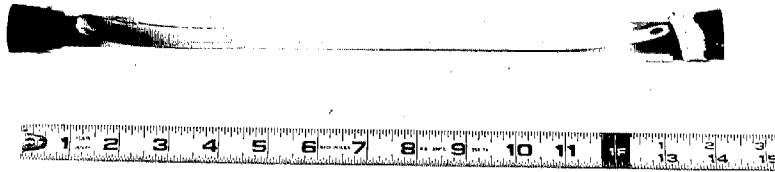


Figure 8  
VIEW OF THE SAMPLER ASSEMBLED AND  
IN SAMPLING ARRANGEMENT



H26089

Figure 9  
VIEW OF AN ALUMINUM-MYLAR COLLECTOR  
STRIP IN ITS GLASS CONTAINER

conducted by counting strobe mark advances on the face of the sampler at (1) the end of one minute, and at (2) the end of ten minute intervals for 10,000 RPM. Ten minute tests were conducted at 8,000 and 6,000 RPM. The results are shown in Table I. These test data shows a surprisingly good 0.1% or better speed control and selectability. An additional 10,000 RPM test showed an average of 0.041% deviation for three 10 minute runs.

Fig. 10

Circuit Layout for Speed Control Test

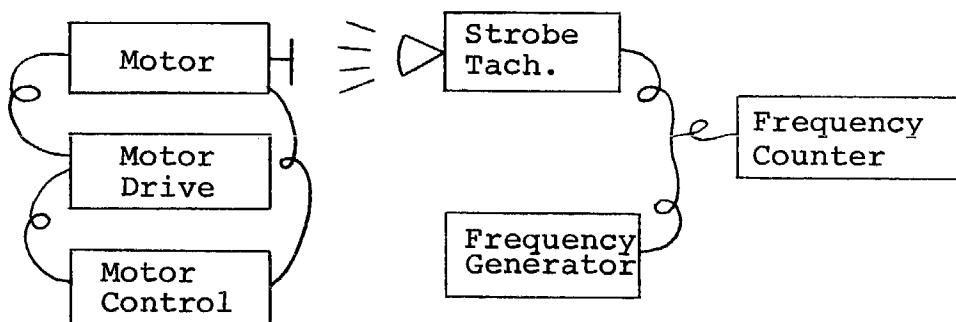


TABLE I

Speed Selectability and Control Test Results

Set Speed RPM	Speed Selectability Test (fast or slow)	% Deviation in 10 minutes	Coefficient of variation, 1 minute inter- vals; N = 10.
10,000	Slow	0.012	0.017
8,000	Fast	0.13	-----
6,000	Fast	0.005	-----

#### 4.0 Split Ratio Determination

The split ratio is defined as the ratio of flow rates between the two streams, the analytical aerosol sample : carrier gas, inside the sampler. This will be expressed as the percentage of the total flow belonging to the analytical aerosol. A relatively high analytical fraction would lead to a desirable shorter sampling time; but the introduction of a large analytical aerosol stream into the laminar process stream generates Coriolis forces and reduces resolution. The optimum split ratio would have a maximum analytical aerosol fraction consistent with acceptable resolution. The split ratio is a function of the depth of the channel cut into the collimating insert. Tests were conducted to determine the split ratio as a function of channel depth.

The tests were static ones in which the sampler was positioned in a test rack. The test arrangement and the method of isolating the analytical stream for its independent measurement is depicted in Fig. 11. A small hole was drilled in the bottom of the sampler body at the entry point of the analytical stream. A baffle of aluminum foil forced the analytical stream out the hole into the measuring apparatus rather than joining the carrier gas (see inset in Fig. 11). The carrier gas exited, and its volume measured, by way of the sampler's exit orifice at the end of the annulus. These two independent lines with pressure gauges and rotameters were subsequently joined and connected to a common vacuum source. A preliminary test indicated that the sensitivity

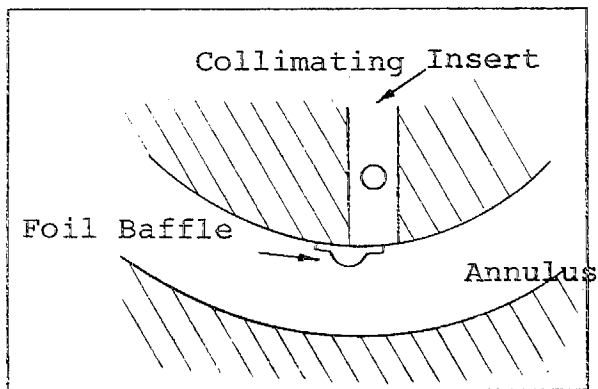
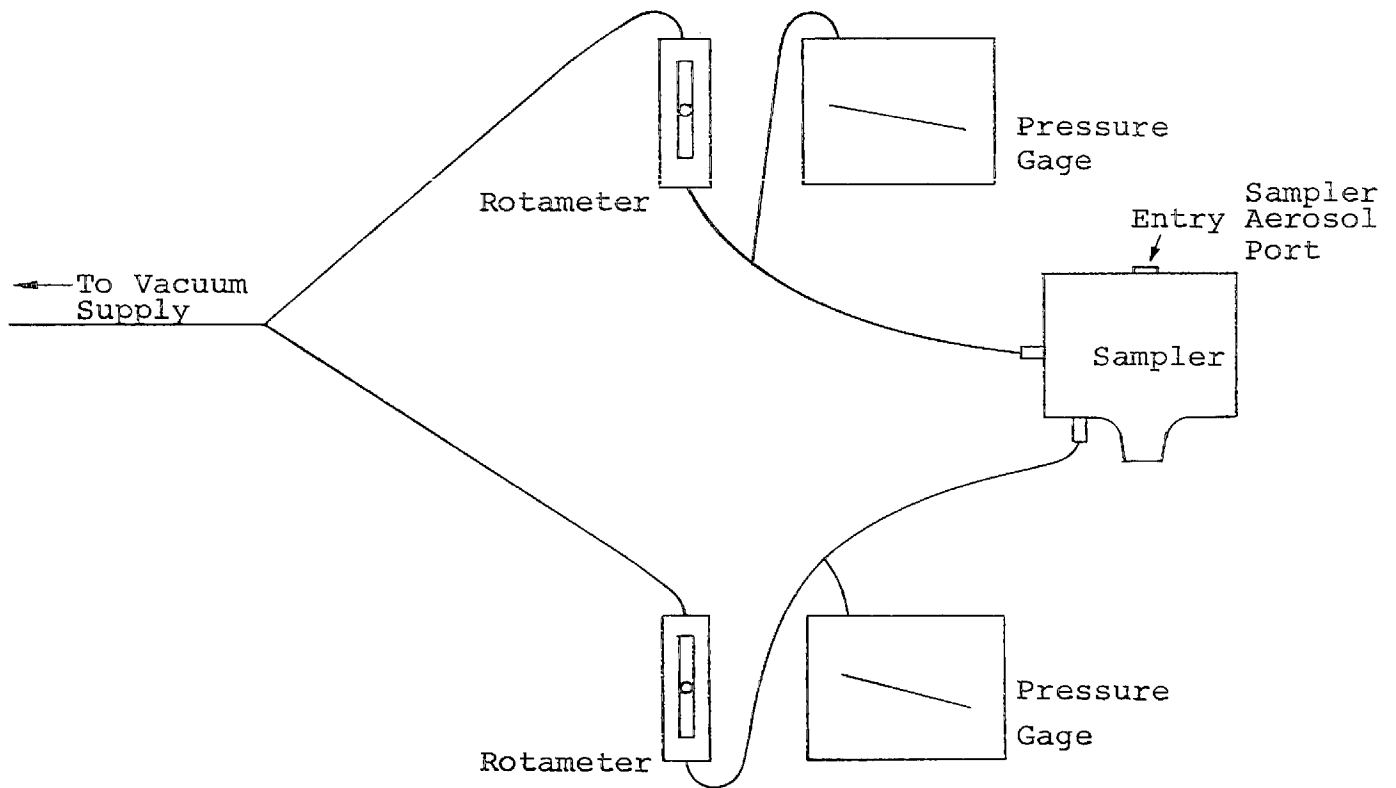


Fig. 11

The upper diagram shows the testing arrangement for the split ratio determination. The lower-left inset shows a sketch of the area in the sampler where the two streams join and the method used for isolating the analytical stream for measurement.

of the pressure gauges would cause no more than 1% error in measuring flow rates.

The tests were run using an expected operating total flow rate of 12 ml/sec. The exit for the carrier gas was equipped with a limiting orifice of 0.029", an expected operating orifice size. Three collimating insert depths were tested. Several runs with each insert resulted in the following data:

<u>Depth of Channel in Collimating Insert, mm</u>	<u>Percentage of Total Flow in Analytical Stream</u>
0.25	28
0.18	16
0.11	10

From these data the plot shown in Figure 12 can be used to determine the split ratio when subsequent resolution tests defines the accepted channel depth.

Also, as a result of these tests it was determined that the differential operating pressure inside the sampler is 0.5 to 0.6 mm Hg. This suggests the particles will not be subjected to significant pressure differential during sampling. It is also worth noting that at a flow rate of 10 ml/sec. the linear particle velocity in the annulus is approximately 10 cm/sec (0.33 ft/sec.). These data are indicative of a very passive deposition environment.

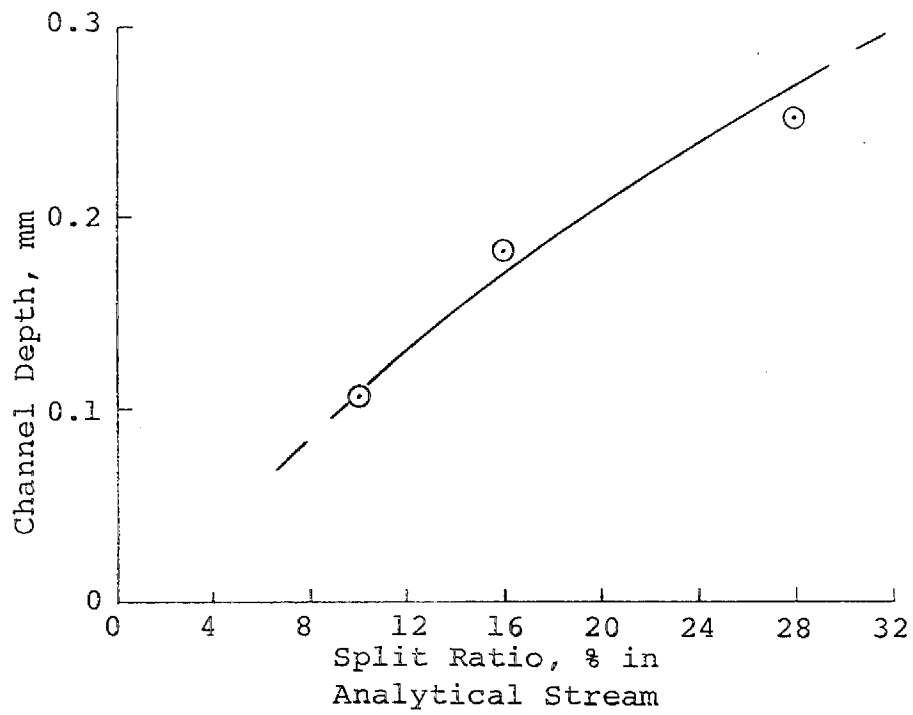


Fig. 12

Plot of split ratio versus channel depth in the collimating insert.

## 5.0 Calibration

After balancing, experiments were begun to determine calibration functions: i.e., outlet orifice size (exact flow rate) and resolution (collimating insert channel depth). These runs were made by sampling a monodisperse aerosol of polystyrene latex microspheres. The aerosol generator is described in Appendix B.

The generation of such an aerosol results in a series of equivalent aerodynamic particle sizes represented by singlets, doublets, triplets, etc. of unit microspheres. The centrifuge sampler deposits these equivalent sizes as a spectral series. The equivalent size, as a function of aggregate number, is known (Ref. 2). An approximation of the required outlet orifice size was first made. Repeated runs with various sized outlet orifices led to an approximate calibration.

With the approximate calibration, resolution studies defined the optimum channel depth in the collimating insert. Resolution is indicated by the width on the collector strip over which a given sized particle is deposited. In addition, the presence of significant Coriolis forces is suggested by the shape of the deposition pattern. High resolution and minimum Coriolis forces would yield a straight and narrow deposition pattern across the width of the collector strip. The quantitative measure of resolution used is

$$R\% = \frac{W}{S} \times 100 \quad (\text{Eq. 4})$$

R% - Resolution as a percentage of S

s = particle size in  $\mu\text{m}$

w = visible deposition line width converted to micrometers by the samplers calibration

An aerosol of 0.500  $\mu\text{m}$  polystyrene was sampled successively using the three collimating inserts with increasing channel depths. The data obtained are shown in Table II.

These experiments showed that a resolution of 5% is achieved with a collimating insert of 0.11 mm. Referring to the graph in Figure 12 Section 4.0 it is seen that a 0.11 mm insert channel depth yields a 10% split ratio.

With the above parameters defined the final calibration experiments were conducted. This included three separate runs using successively larger, 0.234  $\mu\text{m}$ , 0.500  $\mu\text{m}$ , and 1.30  $\mu\text{m}$ , polystyrene microspheres. In each case the synthetic aerosol was sampled long enough to collect visible deposition lines of the aggregate series in the form of a spectral distribution. The calibration is defined by measuring the millimeter location on the collector strip at which particles of a known equivalent aerodynamic size occurred. The data obtained are listed in Table III. Figure 13 shows a plot of the calibration. On the graph the horizontal width of the points represents the approximate width of the visible deposition zones. The vertical height of the points represent the stated accuracy of the polystyrene sizes. The sizing accuracy of the centrifuge is therefore suggested by these extremes. The collection width for the 0.234  $\mu\text{m}$  singlets was 85 to 105 mm. The sampler's dispersion in this size range

yields the micrometer range for this deposition zone to be 0.240 to 0.220  $\mu\text{m}$  (+0.006 to -0.014  $\mu\text{m}$ ). By equation 4 this is 3% to 6%. A similar resolution was found for the 0.500  $\mu\text{m}$  singlets. The deposition zones were narrow, nearly straight and verticle to the collector strip's length indicating little turbulence or Corolis forces during deposition. The aggregate number in each of the deposition lines was confirmed by scanning electron microscopy. An example of an aggregate spectral series is shown in Figures 14 through 17 for the singlets through quadruplets of 0.500  $\mu\text{m}$  unit spheres. Figure 18 shows a complex aggregate of 0.234  $\mu\text{m}$  spheres. Figure 19 shows a giant aggregate of 0.234  $\mu\text{m}$  spheres photomicrographed at  $\sim 3\text{mm}$  on the collector strip.

A second, though tentative, calibration was formed for a larger particle size range. The rotational speed of the sampler was slowed to minimize entry losses of large particles, and the exit limiting orifice was proportionally increased to provide an appropriate flow rate. At 2,000 RPM and 0.052" exit orifice spectral distributions were obtained on 1.09  $\mu\text{m}$  and 2.02  $\mu\text{m}$  polystyrenes as listed in Table IV.

Figure 20 shows these data plotted with the previous calibration. This change in sampler parameters to form a different calibration demonstrates the flexibility of the sampler. Discussion in subsequent sections of this report refer to the calibration on the smaller particles as "A" and to the coarser, tentative calibration, as "B".

TABLE II

Data on Resolution Experiments

Run	Channel Depth, mm	Line Width, mm	Equivalent $\mu\text{m}$ Line Width	Resolution, % (from Eq.)
1	0.10	1.0	0.015	3
2	0.18	6.5	0.09	18
3	0.25	$\sim 8.5^*$	0.14	28

\*The singlets line overlapped the doublets line and so this value is estimated.

TABLE III  
Calibration Data

Sphere Unit Size, $\mu\text{m}$	Aggregate Number <sup>1</sup>	Equivalent Size Factor <sup>2</sup>	Equivalent Aerodynamic Diameter, $\mu\text{m}$	Collector Strip Location, Millimeters
1.30	2	1.18	1.58	3.5
1.30	1	1.00	1.30	4.5
0.500	6	1.65	0.825	9.2
"	5	1.54	0.770	10.7
"	4	1.46	0.730	11.4
"	3	1.33	0.665	13.5
"	2	1.18	0.590	17.5
"	1	1.00	0.500	23.5
0.234	5	1.54	0.360	43.0
"	4	1.46	0.342	47.0
"	3	1.33	0.311	57.0
"	2	1.18	0.276	71.0
"	1	1.00	0.234	93.0

<sup>1</sup>Number of units comprising one particle.

<sup>2</sup>From "The Aerodynamic Diameter of Aggregates of Uniform Spheres," W. Stober, A. Berner, and R. Blaschke, Jrl. Colloid and Interface Science, Vol. 29, No. 4, April 1969.

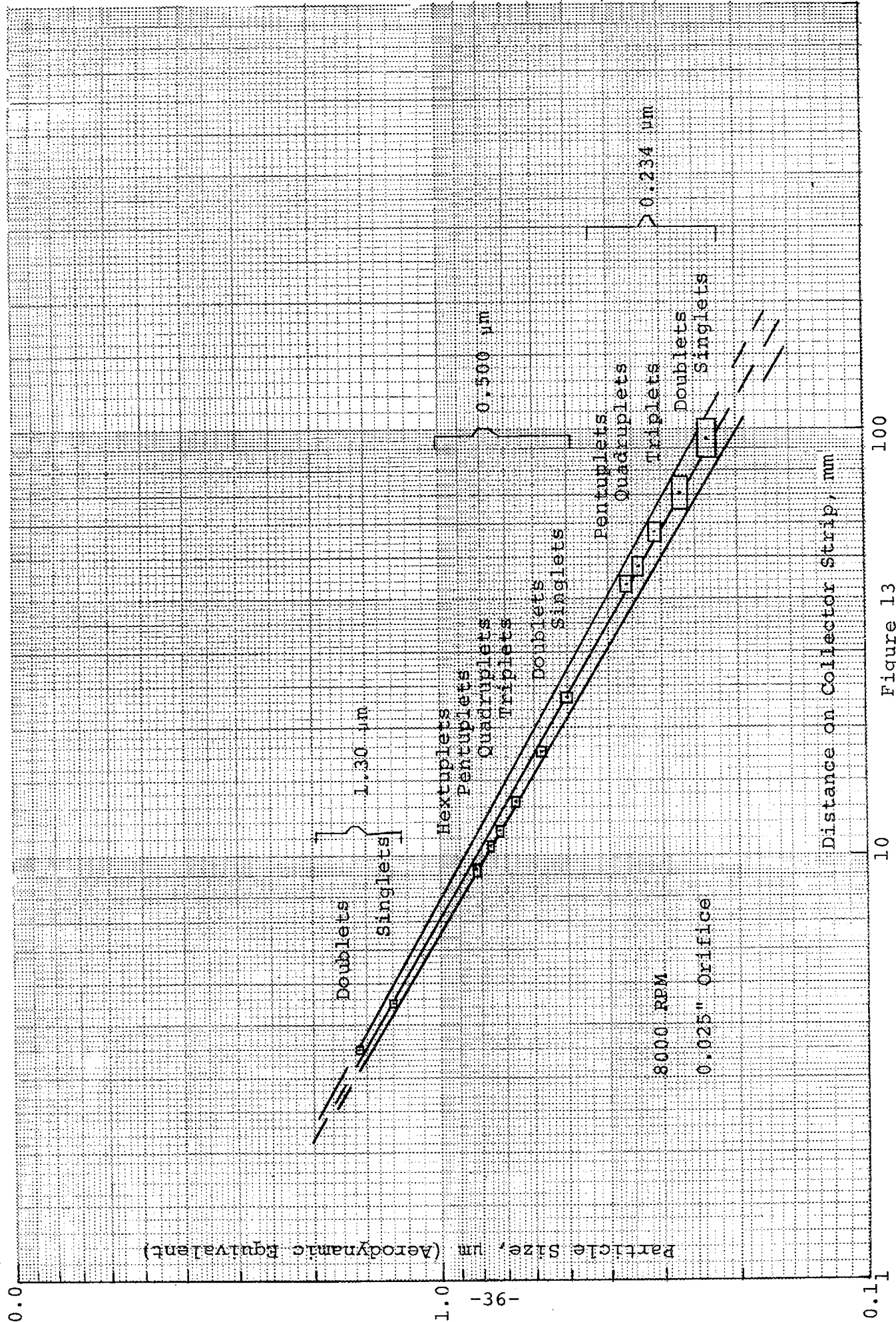
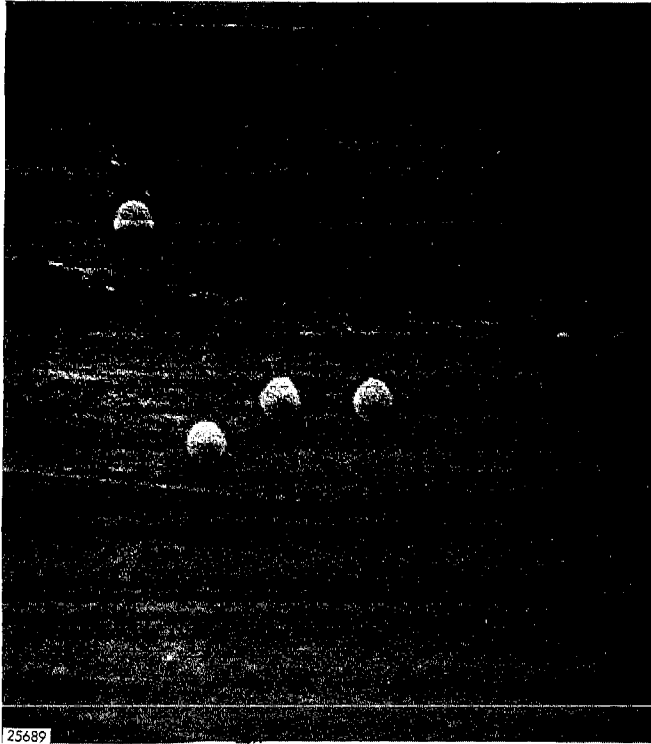


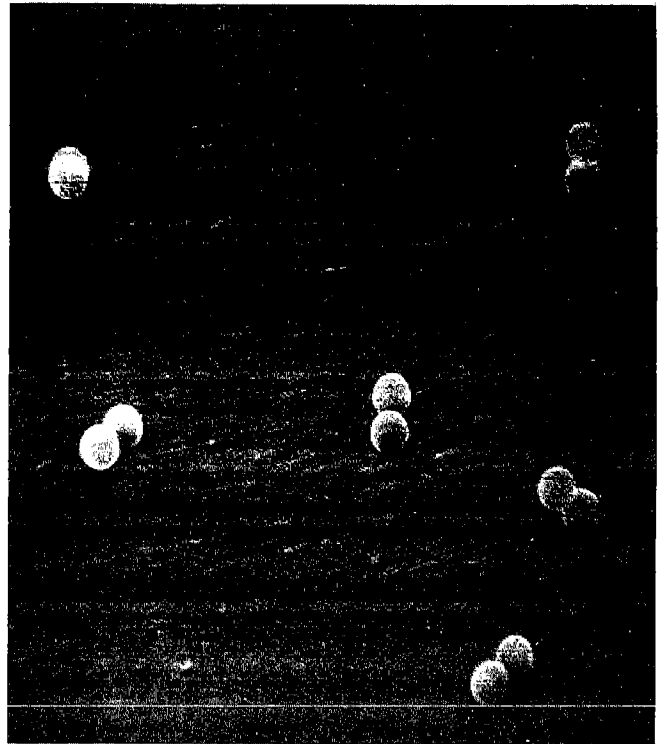
Figure 13

Calibration for Fine Particles



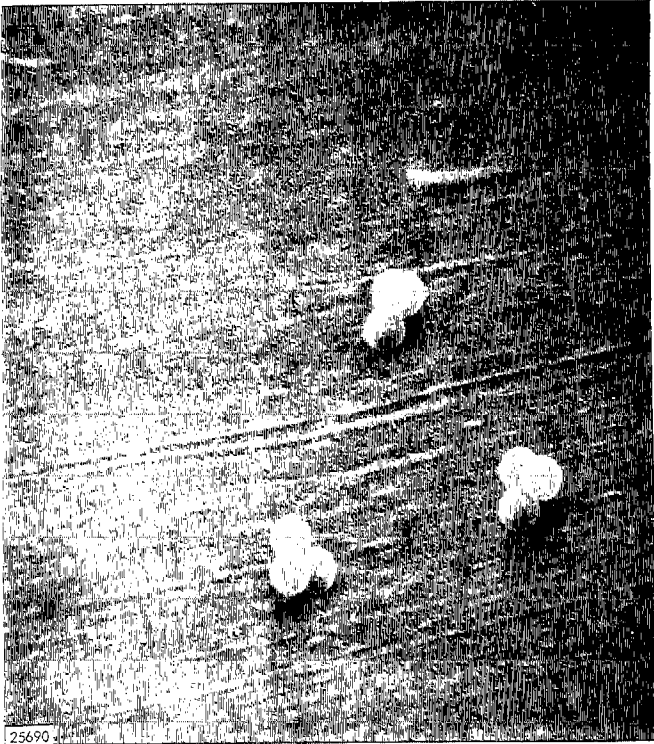
10,000X

Figure 14  
0.500  $\mu$ m SINGLETs OBSERVED AT  
23.5 mm ON THE COLLECTOR STRIP



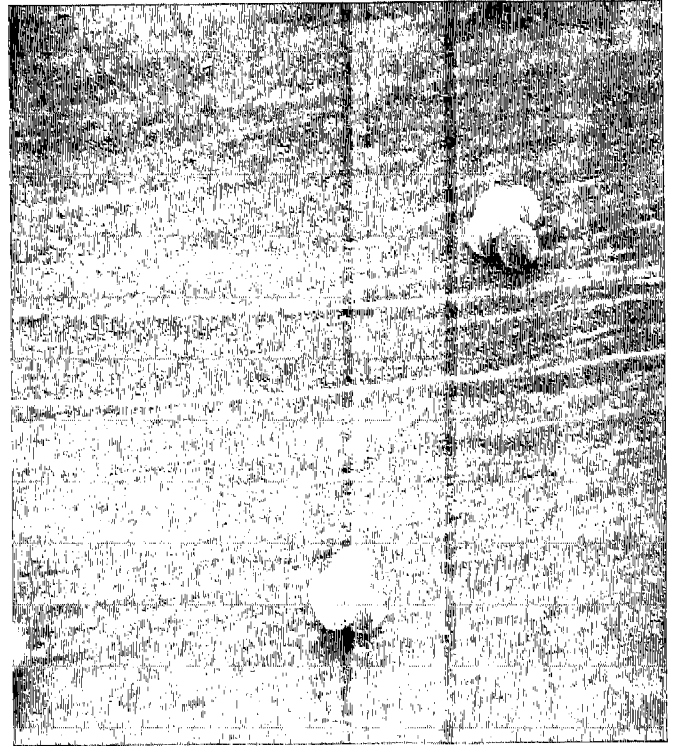
10,000X

Figure 15  
0.500  $\mu$ m DOUBLETs OBSERVED AT  
17.5 mm ON THE COLLECTOR STRIP



10,000X

Figure 16  
0.500  $\mu\text{m}$  TRIPLETS OBSERVED AT  
13.5 mm ON THE COLLECTOR STRIP



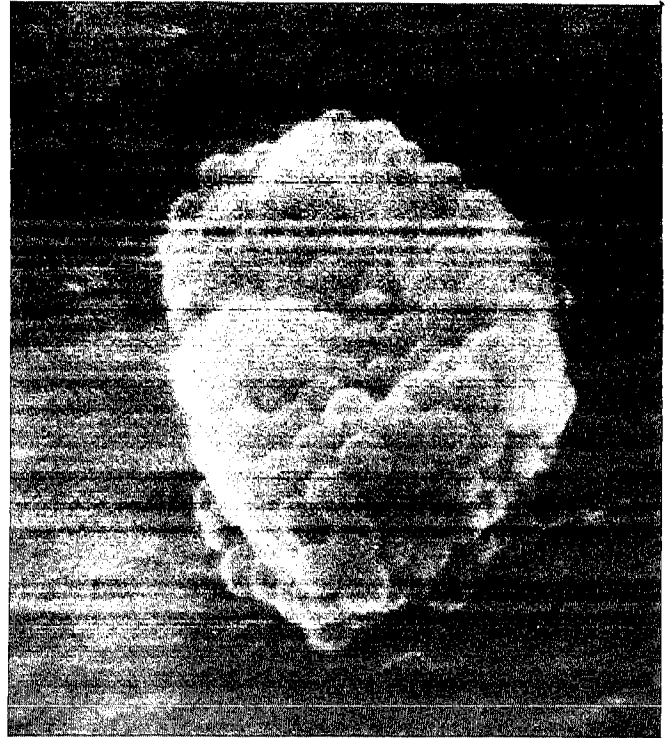
10,000X

Figure 17  
0.500  $\mu\text{m}$  QUADRUPLETS OBSERVED  
AT 11.4 mm ON THE COLLECTOR  
STRIP



30,000X

Figure 18  
COMPLEX AGGREGATE OF  $0.234 \mu\text{m}$   
MICROSPHERES OF  $0.45 \mu\text{m}$   
EQUIVALENT AERODYNAMIC DIAMETER



30,000X

Figure 19  
GIANT AGGREGATE OF  $0.234 \mu\text{m}$   
MICROSPHERES OF ABOUT  $1.6 \mu\text{m}$   
EQUIVALENT DIAMETER

TABLE IV  
 Calibration Data For Coarse Particles

Sphere Unit Size, $\mu\text{m}$	Aggregate Number	Equivalent Size Factor	Equivalent Aerodynamic Diameter, $\mu\text{m}$	Collector Strips Location, mm
1.09	1	1.00	1.09	134
	2	1.18	1.29	95
	3	1.33	1.45	72
	4	1.46	1.59	60
2.02	1	1.00	2.02	41
	2	1.18	2.36	29
	3	1.33	2.66	23
	4	1.46	2.92	19

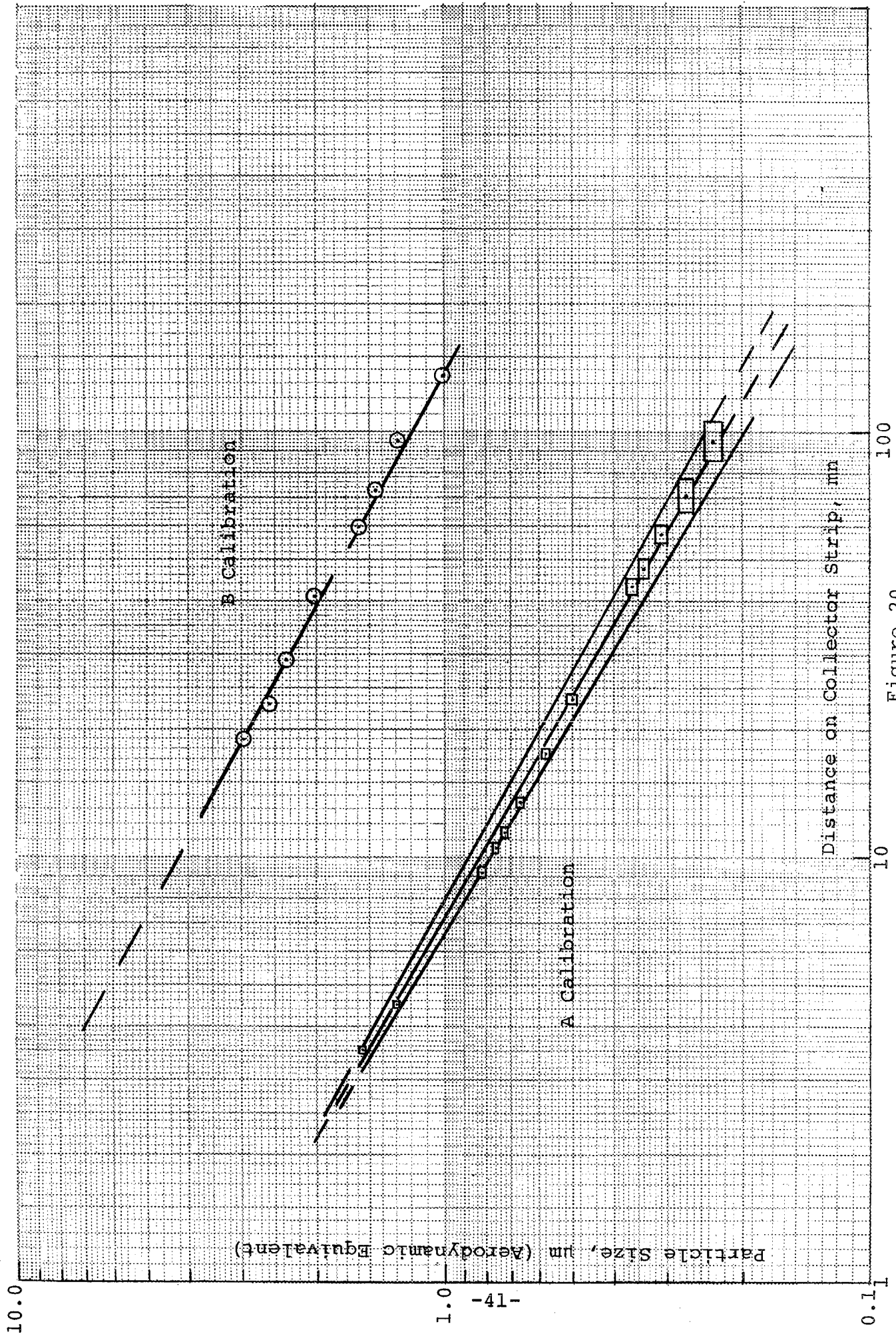


Figure 20  
 Calibration for Fine and Coarse Particles

With the calibrations established the modeling equation (Eq. 3) was used to calculate the flow rates for these calibrations. These calculations found 8.0 ml/sec for "A" and 12.1 ml/sec for calibration "B".

## 6.0 Entry Loss Determination

At the high rotational velocity of the sampler there will be a size-dependent loss of particles in the entry passage ways of the analytical aerosol. These include the analytical tube and the face of the collimating insert. Loss will depend on the particle residence time in those two passages. The loss may be estimated by considering:

$$t = \frac{l}{v} \quad (\text{Eq. 5})$$

t = residence time

l = channel length

v = particle velocity

and 
$$\frac{\Delta T}{t} = \frac{\rho D^2 V^2 \pi N}{18 \eta} \quad (\text{Eq. 6})$$

a form of the Stokes equation in which

$\Delta T$  = transverse particle displacement

t = residence time

$\rho$  = particle density

V = particle velocity

N = sampler angular velocity

$\eta$  = viscosity coefficient of the medium

Equations 5 and 6 can be combined to yield

$$\Delta T = \frac{\rho D^2 \pi N l}{9 \eta} \quad (\text{Eq. 7})$$

This is the thickness of the layer from which all particles larger than D are deposited. The percentage loss is then

$$L\% = \frac{\Delta T}{T} \times 100 \quad (\text{Eq. 8})$$

T = channel depth

Solutions to these equations predict that at 8000 RPM the analytical tube would theoretically remove 1.5% of 0.5  $\mu\text{m}$  particles, 6% of 1.0  $\mu\text{m}$  and 13% of the 1.4  $\mu\text{m}$  particles. The face of the collimator would theoretically remove 5% of the 0.5  $\mu\text{m}$  particles, 34% of the 1.0  $\mu\text{m}$  particles, and 76% of the 1.5  $\mu\text{m}$  particles. The expected combined effects are

<u>Size</u>	<u>% Loss</u>
0.5 $\mu\text{m}$	5 + 1.5 = 6.5
1.0 $\mu\text{m}$	34 + 6.0 = 40%
1.5 $\mu\text{m}$	76 + 13 = 89%

It is obvious that entry losses are significant and increase rapidly with increasing particle size.

The experimental entry losses were determined by sampling with the centrifuge a synthetic aerosol in which the particle size distribution had been determined by independent means. The aerosol was generated by the device described in Appendix B. The starting material for generating the aerosol was a water suspension of a material that is largely iron oxide. This material is a natural residue product from the Bayer process of winning aluminum oxide from Bauxite. The particles of the aerosol from

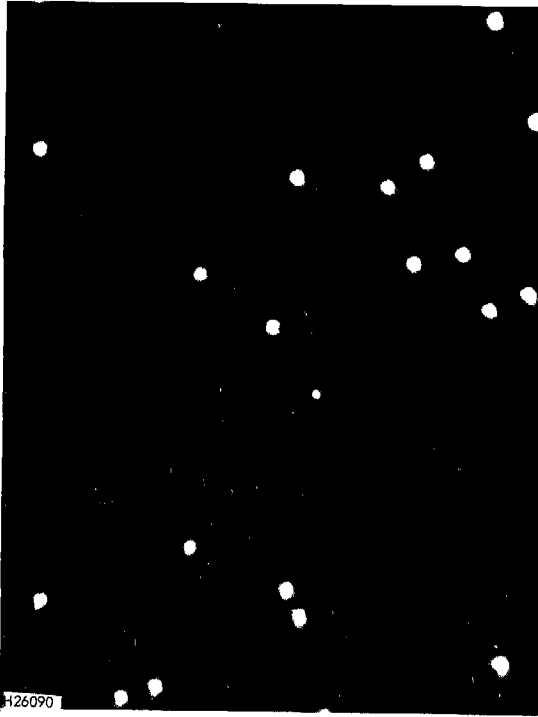
this material are typically subspherical aggregates with a bulk density of near 1.0, a 10-90 size-number percentile range of 0.1 to 1.0  $\mu\text{m}$ . Appendix C comprises a detailed description of the character and the methods of characterizing this material. The characterization methods included (1) air sedimentation with electron microscope sizing and counting, and (2) sampling and collecting with a Brink Cascade impactor and calculation to a number distribution.

The size distribution of the synthetic aerosol as expressed by the centrifuge sampler was made by counting particles at selected locations on the collector strip. For this analysis the collector strip was black varnished paper and the particle counts were made by dark field optical microscopy. In dark field the deposited particles were easily counted because they appear as bright spots on a black background. Because of the high contrast, counts can be conveniently made on particles as small as 0.4  $\mu\text{m}$ . Figure 21 shows an example of the microscope view with this method on 1.0 to 0.5  $\mu\text{m}$  particles.

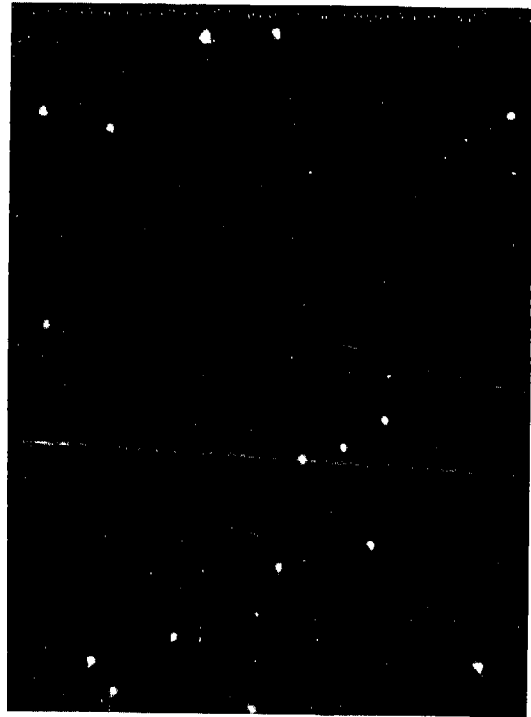
The number of particles present at selected positions on the collector strip (size) were determined on duplicate samples down to 0.4  $\mu\text{m}$ . The calculated theoretical loss at 0.4  $\mu\text{m}$  is less than 3% and are assumed to be negligible. Table V shows this number-size distribution data as a sum from the two runs with the data normalized to 1000 particles at 0.4  $\mu\text{m}$ .

These data are compared to the size-number distribution data by the independent analyses (from Appendix C) as graphical plots in Figure 22. A difference curve which expresses percentage

loss as a function of particle size is shown in Figure 23. This curve is used to correct an actual count distribution on the collector strip to a true size distribution.



1.0  $\mu\text{m}$  Particles



0.5  $\mu\text{m}$  Particles 700X

Figure 21  
SYNTHETIC AEROSOL PARTICLES COLLECTED WITH THE CENTRIFUGE  
SAMPLER ON BLACK VARNISHED PAPER AND VIEWED WITH DARK FIELD  
OPTICAL MICROSCOPY

TABLE V

Summary Data of Number Distribution  
by Centrifuge Sampler

Particle Size, $\mu\text{m}$	Particle Count Normalized to 1000 at 0.40 $\mu\text{m}$
1.5	2.6
1.4	7.8
1.3	23.0
1.2	43.0
1.1	70.0
1.0	137.0
0.9	230.0
0.8	390.0
0.7	590.0
0.6	775.0
0.5	860.0
0.4	1000.0

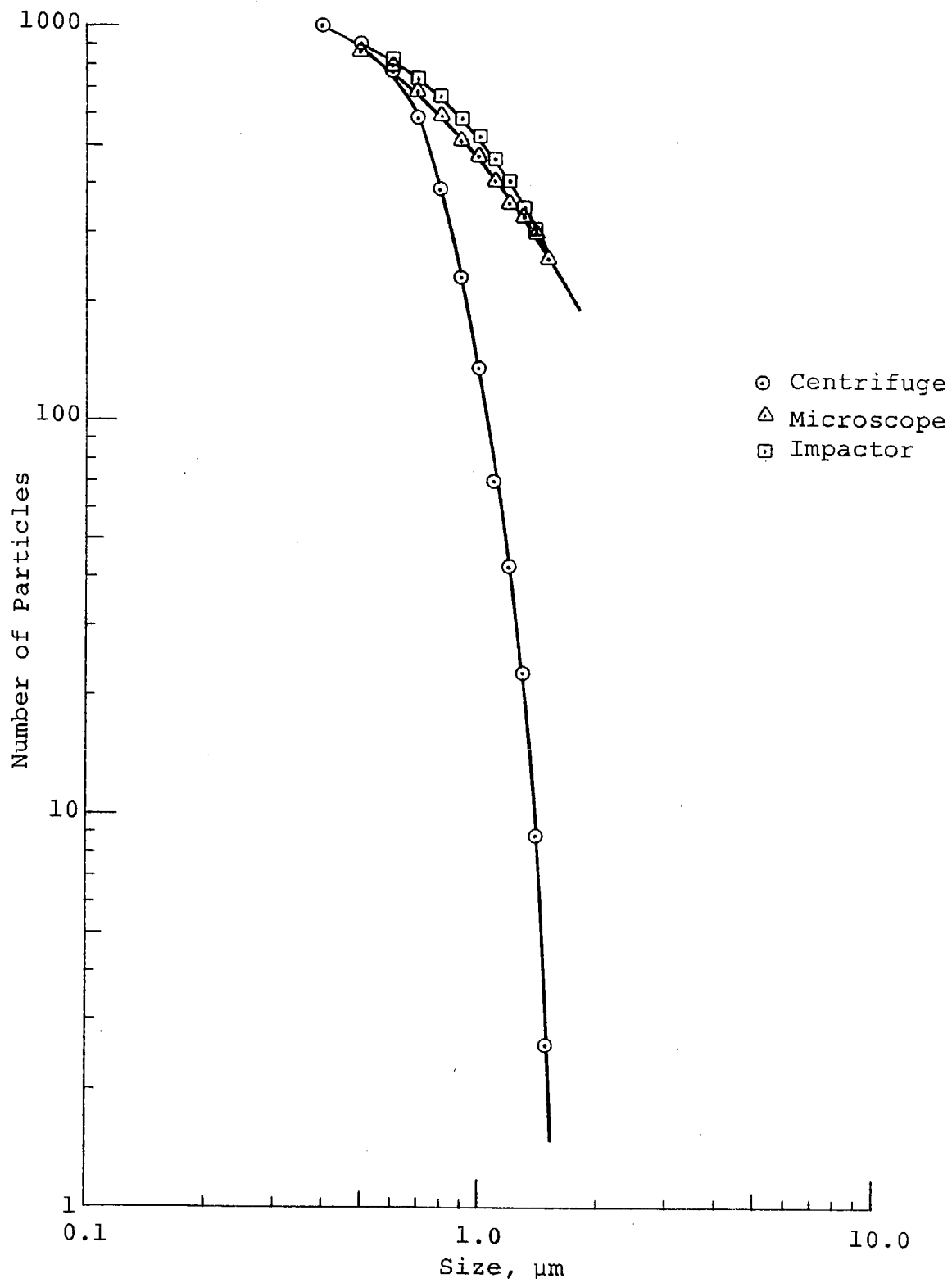


Figure 22  
 NORMALIZED NUMBER-SIZE DISTRIBUTIONS

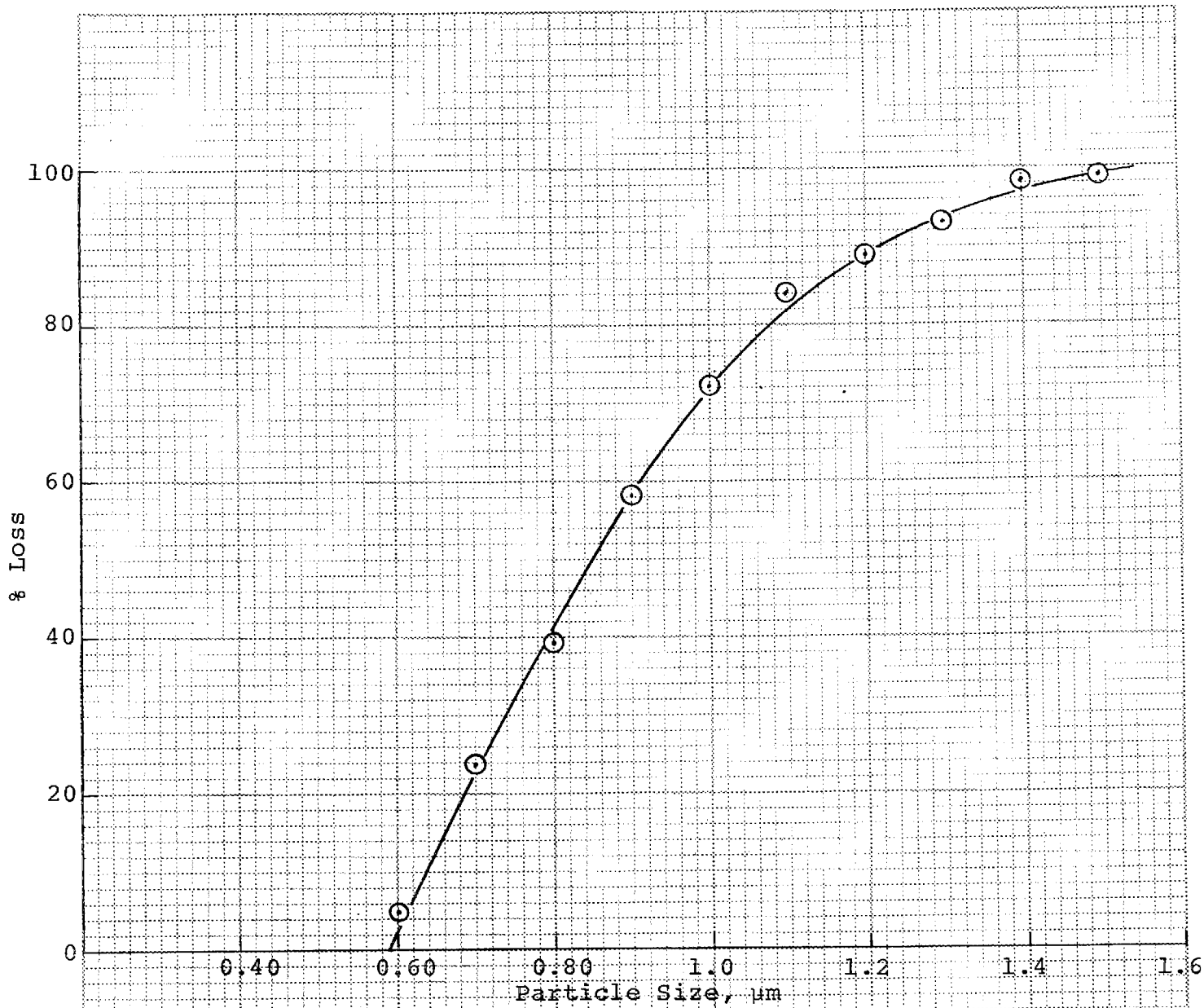


Figure 23  
ENTRY LOSS CURVE

## 7.0 Sampling and Results

### 7.1 Preliminary Field Tests

The first ambient air sample was taken at CFT on the roof of A-building. The objectives in this test were to 1) confirm the possibility of unattended operation of the sampler during a prolonged sampling period (24 hours), 2) gain experience in loading and unloading the mylar aluminum collector strips in a contamination free manner, 3) gain experience in the use of the collector strip containers, 4) develop methods in measuring, sectioning, mounting and otherwise preparing the specimens for electron microscopy, and 5) applying the electron microscope to these specimens. This run proved successful and provided useful experience in developing the many manipulative skills and techniques.

The second run was made in Oakland on July 9-10. This was a 24 hour sample run on the roof of the State Office Building in connection with Air Resources Board's Oakland monitoring station. The microscope results from this run confirmed an earlier suspicion that the spectral distribution was being contaminated by a leak in the precleaner section. The leak was traced to the seal on the web between the leading and the trailing channels in the precleaner section. Steps were immediately taken to correct the problem. A verticle slot was machined in the center of the web. The slot was fitted with a teflon bar. Centrifugal force of the sampler moves the teflon bar out against the wall of the cap and forms a tight seal.

These preliminary field runs had provided experience in operating the samplers, handling the resulting samples, and lead to the correction of a design deficiency.

## 7.2 Samples From Pomona, California

During the week of August 20-25 samples were taken at Pomona, California. The sampling point was on the roof of the ARB's mobile monitoring station which was then located at the Los Angeles County Fairgrounds.

Figure 24 shows a calendar schedule of the samples taken. Sample identification numbers, the calibration range, type of collector strip, etc. are all shown on the figure. Sample 767-68-1 and 767-69-2 were delivered to U.C. (Davis) for chemical analyses. Samples 767-69-1, 767-69-2, and 767-67-1 were the subjects of intensive scanning electron microscopic study. Samples 767-70-1 and 767-70-2 used black varnished paper collector strips and are available for particle counting by dark field optical microscopy. In addition, segments of mylar were mounted in various places in the entry passages of the sampler which collected the 767-767-1 (B calibration) sample. Microscopic examination of these specimens will offer a view of the coarsest particles taken in by the sampler as well as a view of some of the "entry loss" particles.

### 7.2.1 Scanning Electron Microscopic Work

Samples 767-69-1 and 767-67-1 were taken simultaneously using the "B" (coarse) and "A" (fine) calibrations. These two time

Monday 8/20	Tuesday 8/21	Wednesday 8/22	Thursday 8/23	Friday 8/24	Saturday 8/25
-------------	--------------	----------------	---------------	-------------	---------------

Sampler #2 767-68-1; 112 hrs, Chemistry (1.5 to 0.15  $\mu$ m)

Sampler #3 767-70-1 (.5-0.15 $\mu$ )  
Paper Collector

767-68-2; 64 hrs, Chemistry  
(1.5 to 0.15 $\mu$ m)

Sampler #4 767-69-1 (1.5-0.15 $\mu$ )  
Mylar for SEM

767-69-2 (1.5-0.15 $\mu$ )  
Mylar for SEM

Sampler #1 767-67-1 (5 to 0.9 $\mu$ )  
Mylar for SEM

767-70-2 (5 to 0.9 $\mu$ )  
Paper Collector

Figure 24  
CALENDAR SCHEDULE OF SAMPLING AT POMONA

correlative samples form a continuous sample through the entire range of the coarse and the fine distributions. Sample 767-69-2 is size correlative but not time correlative with 767-69-1 (fine distribution).

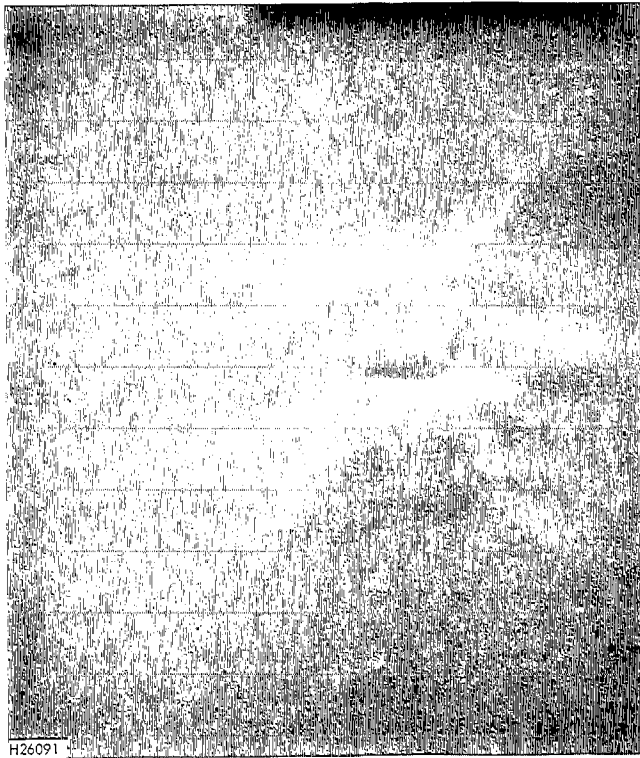
Individual specimens for electron microscopy were prepared by attaching mylar segments to 1/4" diameter SEM sample holder studs with double coated cellophane tape. These mounts were coated with a calculated  $100\text{\AA}$  of Au-Pd by vacuum vapor deposition. The microscope is a Japan Electron Optics Laboratory Co. JSM-U3 unit. The millimeter location included in each specimen was carefully identified.

Samples of blank mylar, i.e., mylar prepared as a collector strip but not exposed, was examined so that typical surface features and contaminant particles could be identified. Also, specimens were prepared from the section of mylar that extended upstream from the analytical zone into the laminating annulus. These samples allowed a view of the very fine particles ( $<0.07\ \mu\text{m}$  for "A" and  $0.4\ \mu\text{m}$  for "B") which penetrate the precleaner. All these specimens provide information on mylar "background".

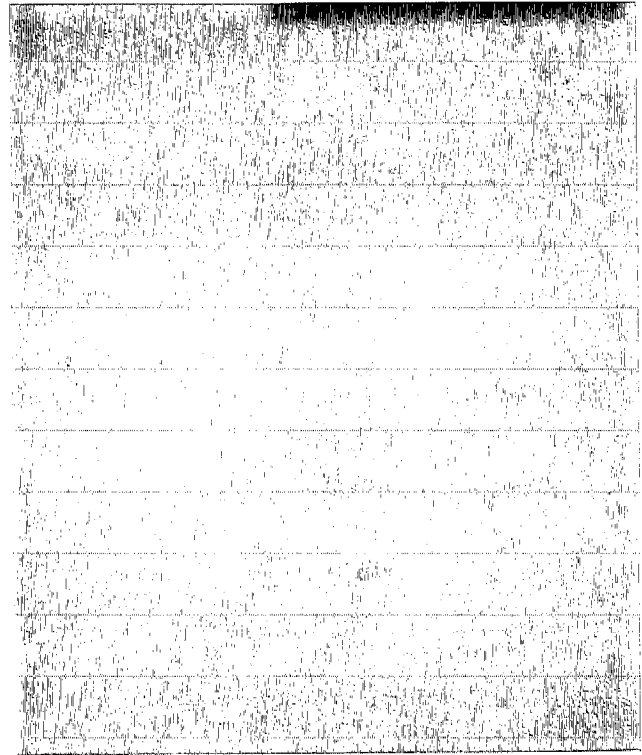
A systematic examination of the spectral and entry zone samples followed. This entailed the detailed examination of 40 individual specimens. In excess of 600 scanning electron photomicrographs were made. The photomicrographs were compiled into an album (Ref. 6). The present report includes copies of a few of the photomicrographs which are particularly demonstrative of particle types, features, and characteristics as a function of size distribution. The reader is referred to the album for full details.

In the systematic microscopic examination the specimen was scanned by the continuous television scanner attachment to the SEM. As particles were intercepted they were photographed or ignored by personal judgement based primarily on two criteria: 1) photograph particles which tend to be representative and exemplary in character and quantity, 2) photograph some particles which tend to be unusual or unique. In most cases a magnification series were taken in order to present detail on an individual particle and also relate it to surrounding particles. Quantitative particle number-size distributions were not attempted. While such is possible and ultimately part of the use of the centrifuge, such work is outside the objectives of the present effort.

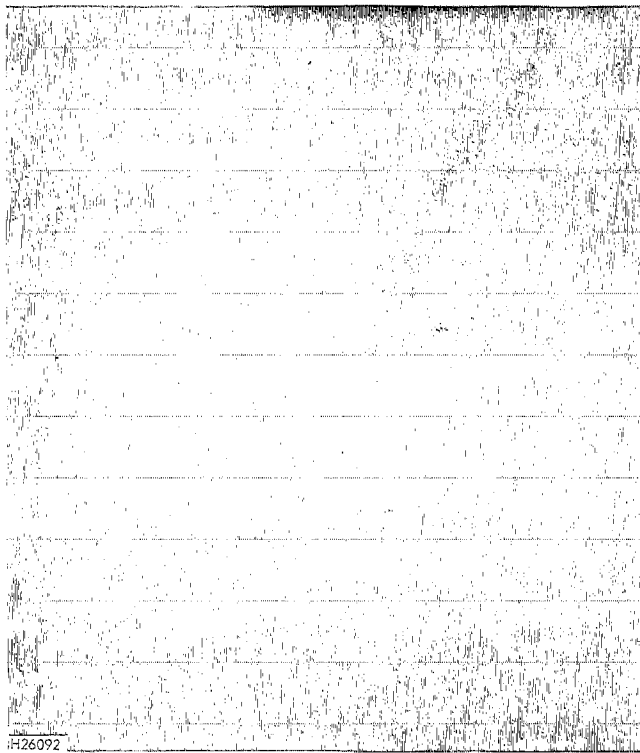
Photomicrographs of the blank mylar surface finds a number of microfeatures, some of which, unfortunately, can be confused with spectrally distributed particles. So far no entirely acceptable material for forming collector strips with SEM in mind has been found. Many materials have been examined and have all been found deficient. Mylar is useable but not ideal. Figure 25 shows an example of blank mylar surface at several magnifications, demonstrating its surface features and some contaminating particles. Figure 26 shows mylar which was taken from the laminating zone, upstream of the analytical zone, with the very small particles which penetrated the precleaner in the "A" (fine) calibration. These particles are theoretically smaller than  $0.07 \mu\text{m}$ . Figure 27 shows "background" mylar from the laminating zone with the "B" (coarse) calibration. These particles which



A. 30,000X

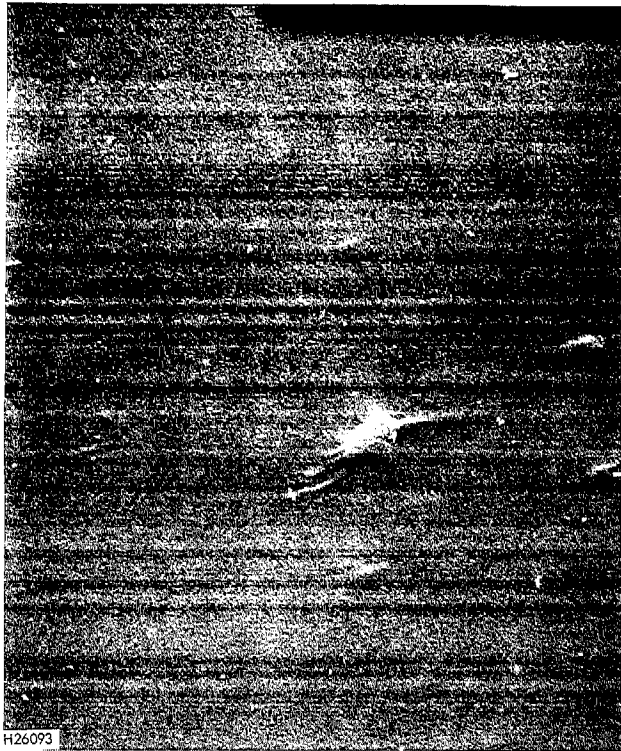


B. 30,000X



C. 3,000X

Figure 25  
BLANK (UNEXPOSED) MYLAR SHOWING  
TYPICAL SURFACE FEATURES AND  
SOME CONTAMINATING PARTICLES



A. 10,000X

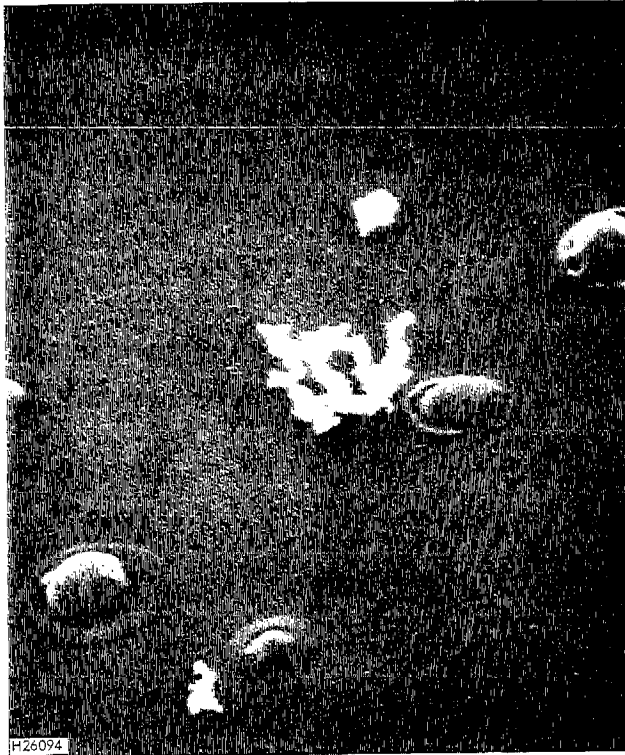


B. 3,000X

Figure 26

MYLAR TAKEN UPSTREAM OF THE ANALYTICAL ZONE IN THE LAMINATING ZONE WITH THE 'A' (FINE) CALIBRATION

Note the small particles which penetrated the precleaner. These particles are theoretically less than  $0.07 \mu\text{m}$  equivalent diameter. The large, centrally located feature is an irregularity in the mylar's surface.



A. 30,000X



B. 10,000X



C. 3,000X

Figure 27  
MYLAR TAKEN UPSTREAM OF THE ANALYTICAL  
ZONE IN THE LAMINATING ZONE OF THE  
'B' (COARSE) CALIBRATION  
These particles are theoretically smaller  
than 0.4  $\mu\text{m}$  and represent particles which  
penetrated the precleaner. The "haloed  
nuclei" in the above example are found  
spectrally distributed in the fine cali-  
bration.

penetrated the precleaner are theoretically smaller than 0.4  $\mu\text{m}$ . This particle type, which I call "haloed nuclei" occurs spectrally distributed in the "A" calibration beginning at about 0.5  $\mu\text{m}$ . These form the dominant number particle type at about 0.35  $\mu\text{m}$  and then become decreasingly prominent at smaller sizes. Figure 28 shows a photomicrograph of "haloed nuclei" as spectrally distributed particles from the "A" calibration. It is interpreted that at the time the sampler sized these particles they occurred as a central nucleating element inside a volatile envelope. They have since been reduced to a residue halo of dissolved solids surrounding the central nucleus.

Figure 29 shows photomicrographs of an aggregate particle type which occurred over the entire range from 8  $\mu\text{m}$  to 0.16  $\mu\text{m}$ . These "grapebunch" aggregates are among the most abundant of all the particle types. They appear with relative increasing frequency in the submicron size range. These particles appear to me to be combustion residue. In no case did this type of particle appear to have a volatile envelope over the entire particle, but always appeared "dusty dry" as in the figure. Within the "grapebunch" type of particle there occurred varieties, subclassed on the basis of the size of the individual units as shown in Figure 30. These subclasses of combustion residue (?) probably are from independent, potentially identifiable sources.

Prominent in the coarse spectrum "B" and in the coarse end of the "A" spectrum were mineral and biological units and fragments. Many of these also occurred in the entry passage ways of



H26096

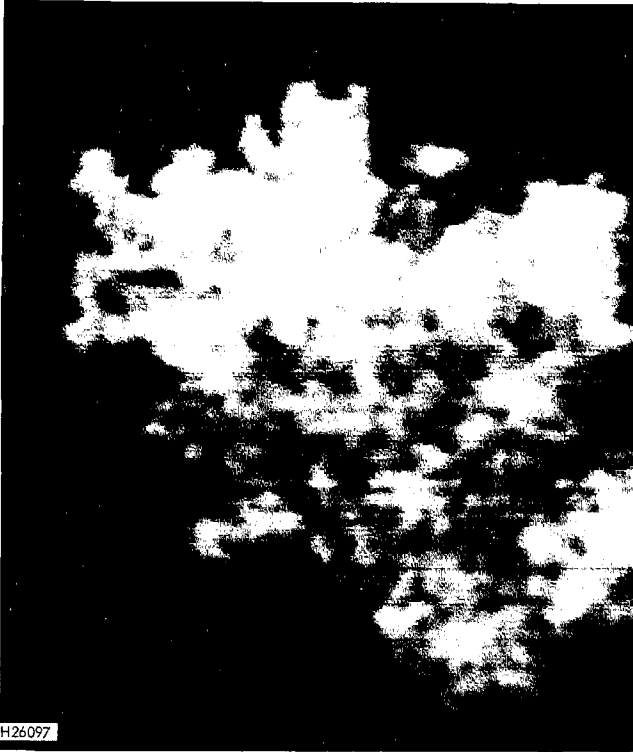
A. 30,000X



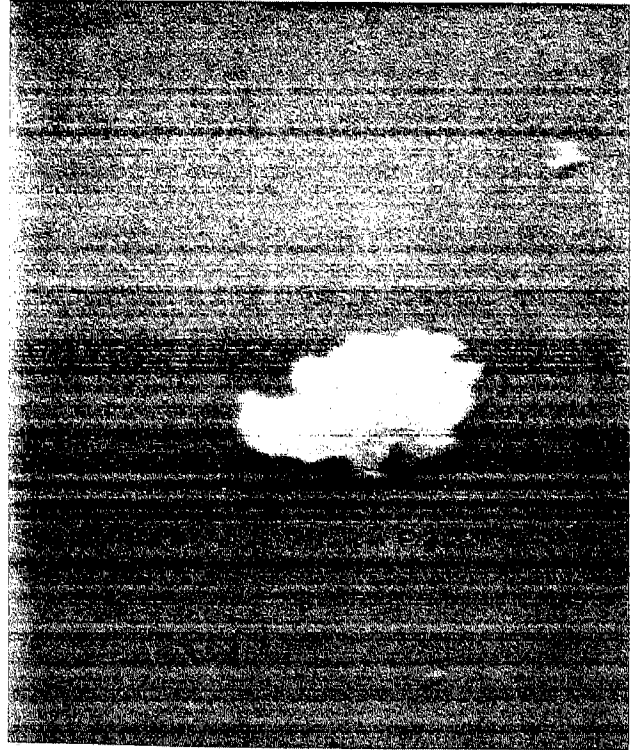
B. 10,000X

Figure 28  
SPECTRALLY DISTRIBUTED "HALOED NUCLEI" FROM THE 'A'  
CALIBRATION OF A POMONA SAMPLE

These particles were of 0.37  $\mu\text{m}$  equivalent aerodynamic size when sized by the spectrometer. The centrally located "grapebunch" particle is the same equivalent size as the "haloed nuclei" originally was.



A. 30,000X



B. 30,000X



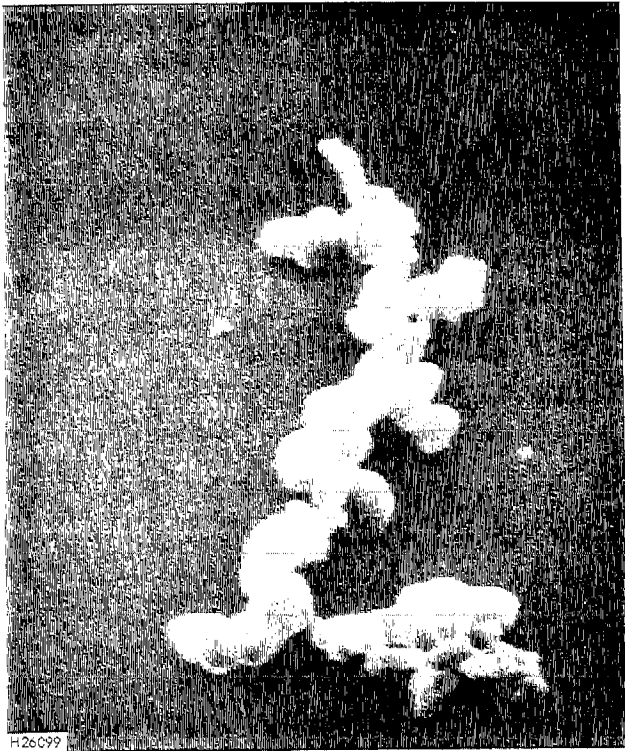
C. 30,000X

Figure 29  
"GRAPEBUNCH" TYPE OF PARTICLE WHICH IS  
THOUGHT TO BE COMBUSTION RESIDUE  
This type of particle occurred over the  
entire range of the two calibrations.

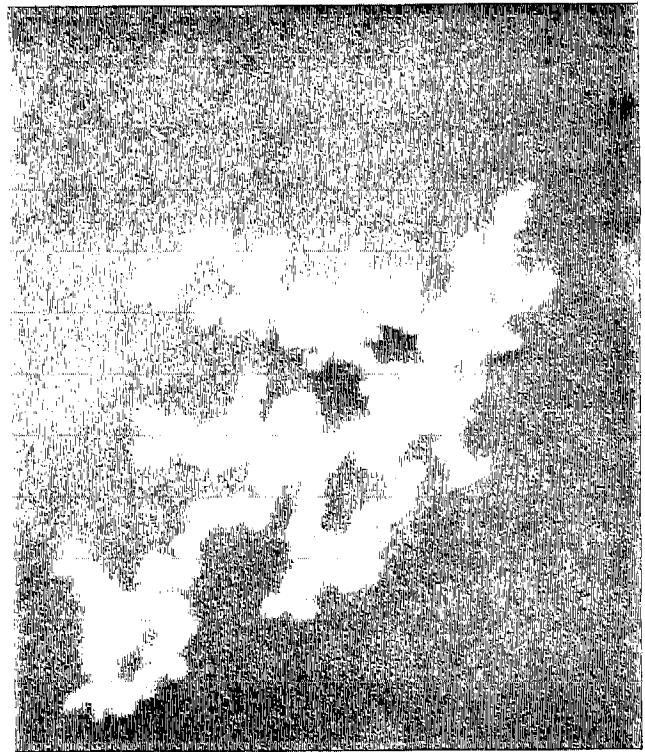
A = 3.9  $\mu\text{m}$  equivalent

B = 0.61  $\mu\text{m}$  equivalent

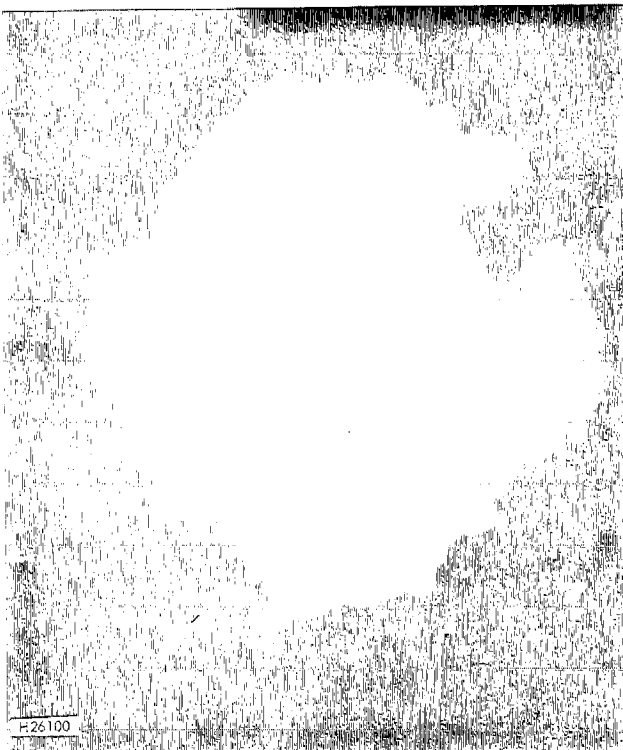
C = 0.16  $\mu\text{m}$  equivalent



A. 30,000X



B. 30,000X



C. 30,000X

Figure 30  
"COMBUSTION RESIDUE (?)" REPRESENTING  
A SUBCLASS SERIES BASED ON THE SIZE OF  
THE BASIC UNIT OF THE AGGREGATES

the sampler. Figure 31 shows examples of biological types; Figure 32 shows examples of mineralogical types of particle.

As a statement of gross patterns it was observed that 1) the entry, nonspectral, portions of the sampler collected material as large as 25  $\mu\text{m}$ , much of which was mineralogical and biological materials, but also included "grapebunch" combustion residue (?) and "haloed nuclei". 2) The coarse "B" spectral distribution included many mineralogical and biological particles and some "grapebunch" particles. 3) With decreasing particle size relatively fewer of the biological and mineralogical particles were observed and the "grapebunch" particles became the dominant particle type in the range of about 1.0 to 0.5  $\mu\text{m}$ . 4) From 0.5  $\mu\text{m}$  to 0.2  $\mu\text{m}$  the "grapebunch" particles were accompanied with a large number of the "haloed nuclei" type. 5) Below 0.2  $\mu\text{m}$  the "grapebunch" particles were again dominant.

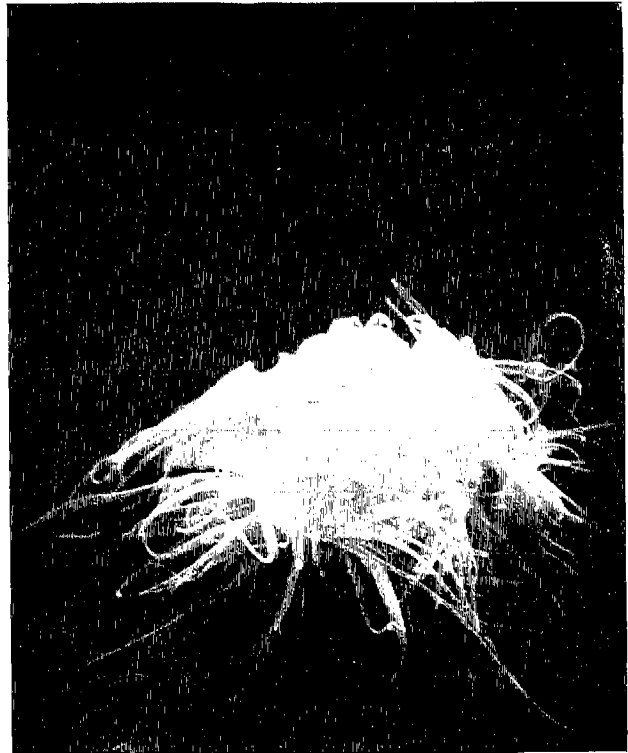
The sampler's modeling equation (Eq. 3) can be reformed to calculate individual particle real density

$$\rho_R = \frac{9nF}{2\pi^2 R_1 D_p^2 Z V^2 C} \quad (\text{Eq. 9})$$

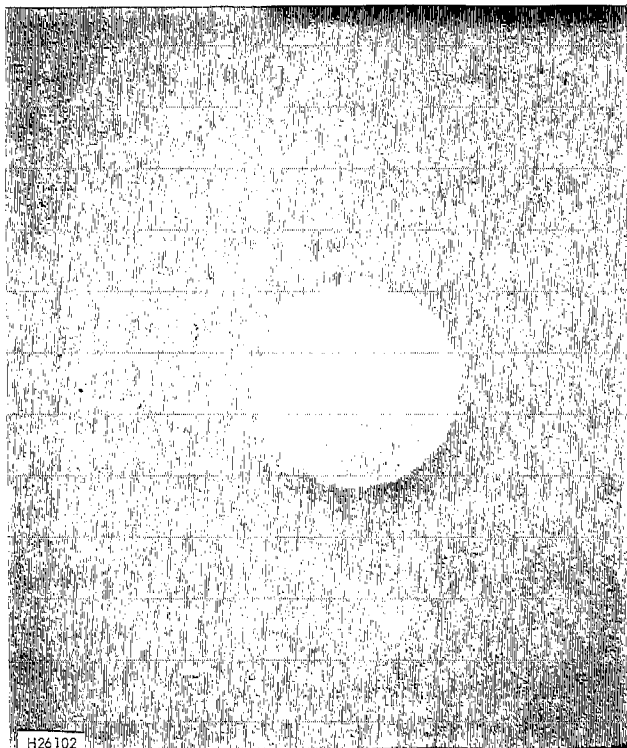
$\rho_R$  is real density. In the case of an aggregate,  $\rho_R$  is real bulk density. During sampling the centrifuge deposited a particle at Z with the defined aerodynamic equivalent density of 1.0 gm/cm<sup>3</sup>. If the particle's physical diameter,  $D_p$ , can be measured from the microscopic image then real density,  $\rho_R$ , can be calculated.



A. 30,000X



B. 5,000X



C. 30,000X

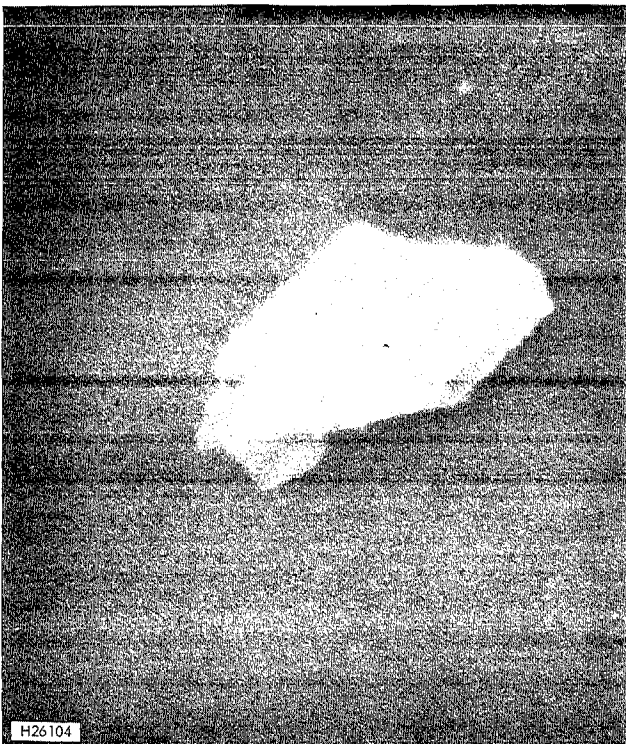
- Figure 31  
PARTICLES OF PROBABLE BIOLOGICAL SOURCE
- A. Spectral size of the aggregate is  $1.10 \mu\text{m}$ . The individual units are about  $0.5 \mu\text{m}$  physical size.
  - B. Collected in the precleaner annulus and not sized. The body of the unit is about  $10 \mu\text{m}$  in diameter.
  - C. Spectral size is  $0.93 \mu\text{m}$ .



A. 20,000X



B. 20,000X



C. 30,000X

Figure 32  
PARTICLES OF PROBABLE MINERALOGICAL  
(NATURAL INORGANIC) SOURCE  
A. Collected in the entry well of  
the precleaner; not sized by the  
centrifuge.

B. 1.4  $\mu\text{m}$  equivalent size.

C. 0.61  $\mu\text{m}$  equivalent size.

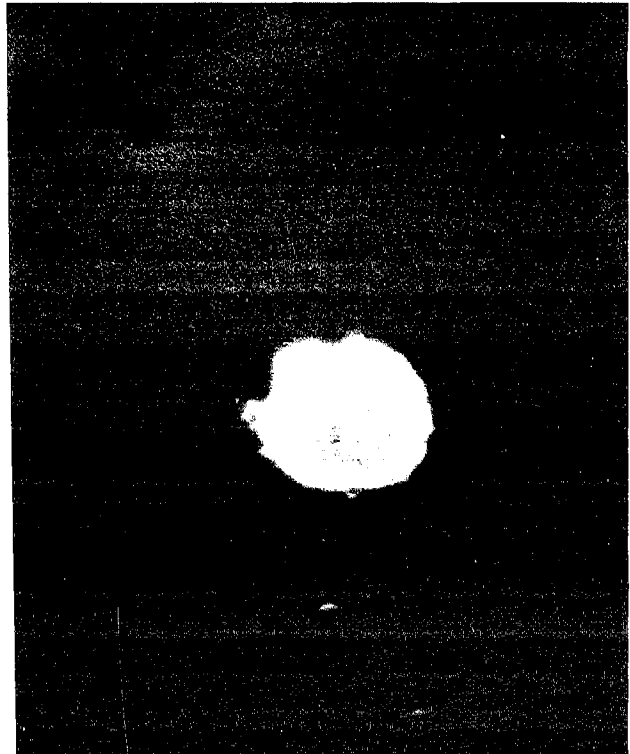
The quality of the calculated density value mainly hinges on the precision with which  $D_p$  can be measured; more limitedly it hinges on particle shape and surface drag. With a smooth equidimensional particle  $\rho_R$  can be calculated to within an estimated 10% of the true value. An irregularly shaped particle could entail considerable error from the measurement of  $D_p$  alone. In some instance there is no sensible way to measure  $D_p$ .

Figure 33 shows photomicrographs of three particles on which density calculations were made. The "grapebunch" aggregate type particle in Figure 33A has a real bulk density of 1.9 gm/cm<sup>3</sup>; the particle in Figure 33B has a calculated 7.6 gm/cm<sup>3</sup>; the particle shown in Figure 33C, of probable biological origin, has a bulk density, including the central hole, of only 0.42 gm/cm<sup>3</sup>. In addition, the spherical "biological" particle shown in C of Figure 31 has a calculated density of 0.25 gm/cm<sup>3</sup>.

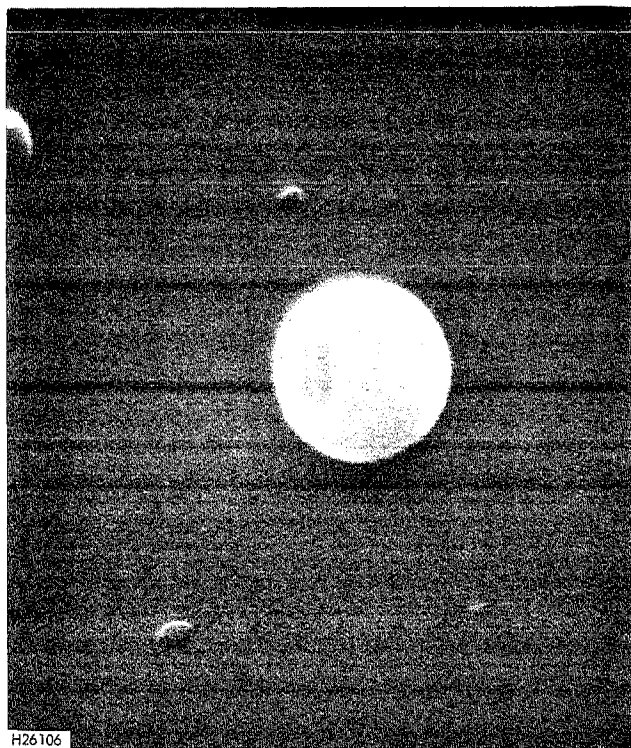
Chemical analyses of the spectrally collected particulate by x-ray spectroscopy has not proved successful. Samples analyzed by the cyclotron source x-ray energy dispersive system at the University of California (Davis) has failed to detect a signal from any element. This failure is rationalized as follows: information on hand for the preparation of the original research and development proposal (Ref. 5) was that the optimum mass on the collector strip for this analytical system was ~15 nanograms/cm<sup>2</sup>. Sampling time estimates were calculated based on that value (p.22) (Ref. 5). The stated sensitivity at present is much different and is listed as ranging from about 100 ng/cm<sup>2</sup> to about 20 ng/cm<sup>2</sup> per element.



A. 30,000X



B. 30,000X



C. 30,000X

Figure 33  
THREE PARTICLES ON WHICH DENSITY  
CALCULATIONS WERE MADE:

A. Equivalent size, 1.15  $\mu\text{m}$ ,  
 $D_p = 1.25 \mu\text{m}$   
 $\rho_R = 1.9 \text{ g/cm}^3$

B. Equivalent size, 0.95  $\mu\text{m}$ ,  
 $D_p = 0.75 \mu\text{m}$   
 $\rho_R = 7.6 \text{ g/cm}^3$

C. Equivalent size, 1.02  $\mu\text{m}$   
 $D_p = 0.73 \mu\text{m}$   
 $\rho_R = 0.42 \text{ g/cm}^3$   
(probably of biological origin)

Considering the nominal concentration of several of the important elements in ambient particulate, the analytical flow rate of the sampler and the area of the collector strip over which the particles are deposited it is concluded that this sampler is incompatible as a sampler for the U.C. (Davis) analytical system. For example, the 112 hour sample at Pomona (767-68-1):

$$1. \quad \left[ 112 \text{ hrs.} \right] \left[ \frac{3600 \text{ Sec.}}{\text{Hr.}} \right] \left[ \frac{0.8 \text{ ml}}{\text{Sec.}} \right] \left[ \frac{1 \times 10^{-6} \text{ meters}^3}{\text{ml}} \right]$$

$$= 0.32 \text{ m}^3 \text{ sampled.}$$

Using a nominal metals concentration for iron ( $4\mu\text{g}/\text{m}^3$ ) and for lead ( $2\mu\text{g}/\text{m}^3$ ) (Ref. 7), and the analytical area of the collector strip:

$$2. \quad \frac{\left[ \frac{(\text{Fe, Pb}) \mu\text{g}}{\text{m}^3} \right] \left[ 0.32 \text{ m}^3 \right]}{(2 \text{ cm}) \times (17 \text{ cm})} = (\text{Fe, Pb}) \times 0.01 \mu\text{g}/\text{cm}^2$$

$$\text{Fe; } (4) \times \frac{0.01 \mu\text{g}}{\text{cm}^2} = \underline{0.04 \mu\text{g}/\text{cm}^2 \text{ metal collected}}$$

$$\text{Pb; } (2) \times \frac{0.01 \text{ g}}{\text{cm}^2} = \underline{0.02 \mu\text{g}/\text{cm}^2 \text{ metal collected}}$$

These mass densities are compared to the sensitivity limits now stated by the U.C. (Davis) people of  $23 \text{ ng}/\text{cm}^2$  for Fe and  $59 \text{ ng}/\text{cm}^2$  for Pb. It is interpreted that for both iron and lead the element mass on the collector strip is about 3 orders of magnitude too low to be detected by the cyclotron x-ray system.

Recent developments in the use of energy dispersive x-ray analytical systems attached to SEM are important. Maggione and Rubin (Ref. 8) describe an optimized SEM unit for chemical analysis

of ultramicroscopic particles. Their device was capable of sensing element x-ray signals on asbestos fibers as small as 500Å (0.05 µm). Because the centrifuge has been demonstrated to collect individual particles remarkably amenable to SEM analysis, chemical information on a particle by particle basis is possible with SEM-centrifuge combination.

### Acknowledgements

The principal investigator wishes to acknowledge the considerable assistance he received during the course of the project. At CFT H. J. Seim and E. O. Strahl provided technical assistance; John Payne provided technical and engineering assistance; J. A. Dickeson provided engineering assistance; J. Balser and Rosa Chau did the electron microscopy. Thanks is given to the Air Resources Board Research Branch Staff including J. Suder, Harris Samuels, and the late Dale Hutchinson for their patience and helpful suggestions.

## References

- (1) Hochrainer, D., "A New Centrifuge to Measure the Aerodynamic Diameter of Aerosol Particles in the Submicron Range", Jol. Coll. & Interface Sci., Vol 36, No2 p. 191, June 1971.
- (2) Stober, W., A. Berner, and R. Blaschke, "The Aerodynamic Diameter of Aggregates of Uniform Spheres", Jol. Coll. & Interface Sci., Vol. 29, No. 4 p. 710, April 1969.
- (3) Stober, W., and H. Flachsbart, "High Resolution Size Spectrometry of Quasi-Monodisperse Latex Spheres with a Spiral Centrifuge", Aerosol Science, Vol. 2, p. 103, 1971.
- (4) Anderson, Paul L., A High Precision Centrifuge-Type Aerosol Spectrometer, Research Report No. CFT RR 72-26, Aug., 1972, Center For Technology, Kaiser Aluminum and Chemical Corp., Pleasanton, CA. 94566
- (5) Anderson, Paul L., A Research and Development Proposal from Center For Technology, Kaiser Aluminum and Chemical Corp., Pleasanton, CA. 94566, August 1972.
- (6) Anderson, Paul L., Scanning Electron Micrographs of Ambient Airborne Particulate Collected with a Centrifuge Aerosol Spectrometer Sampler, A portion of October 1973 monthly progress report ARB Agreement ARB 2-290.
- (7) Cooper, J. A., Review of a Workshop; X-ray Fluorescence Analysis of Aerosols, Battelle Research Center, Seattle, Wash., April 4-6, 1973, p. C-2.
- (8) Maggione, C.J. and F. B. Rubin, Optimization of an SEM Spectrometer System for the Identification and Characterization of Ultramicroscopic Particles, Scanning Electron Microscopy, 1973, (Part I), Proceedings of the Sixth Annual Electron Microscope Symposium, ITT Research Institute, Chicago, Ill. 60616, April 1973.
- (9) Stober, W., and H. Flachsbart, "Size-Separating Precipitation of Aerosols in a Spinning Spiral Duct", Environmental Science and Tech., Vol. 3 p. 1280, Dec. 1969.
- (10) Rabbe, Otto G., "Instruments and Methods for Characterizing Radioactive Aerosols", IEEE Transactions on Nuclear Science, Vol. NS-19, No. 1, Feb. 1972.



APPENDIX A  
BLUE PRINTS AND SPECIFICATION SHEETS

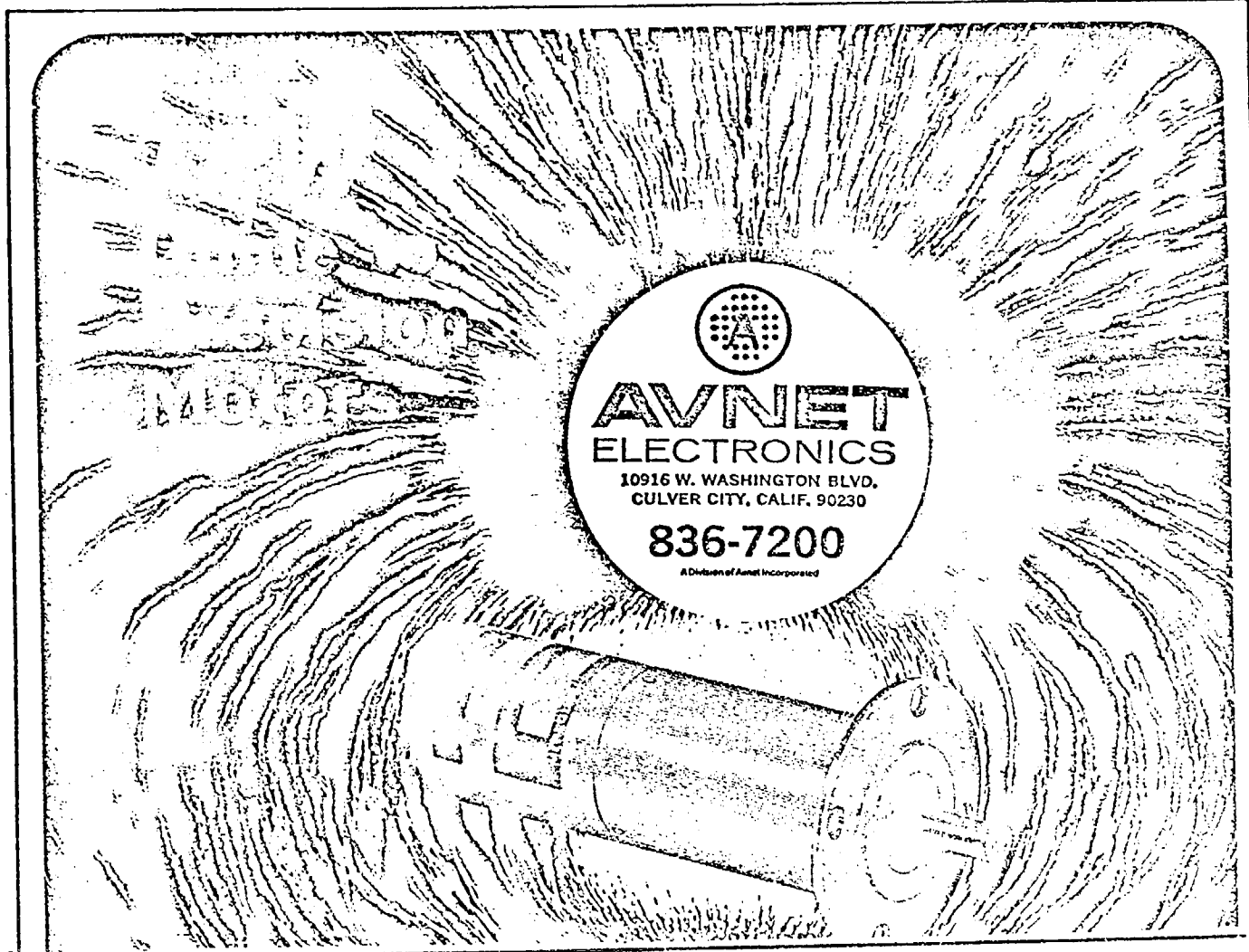
FOR DATA

PLEASE CONTACT

ARB LIBRARY

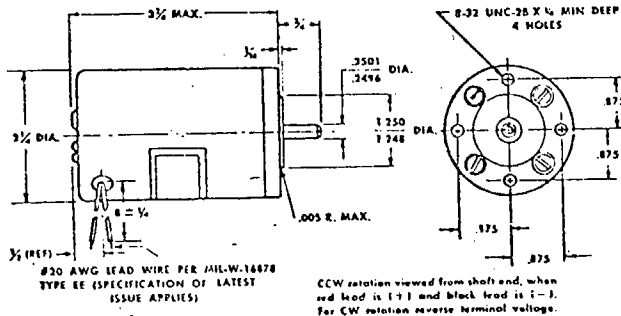
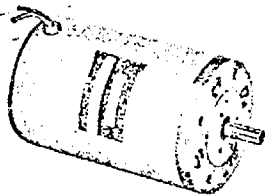
(916) 323-8377

Low S.c.h.m



## D.C. PERMANENT MAGNET MOTORS

### Type GRP (Bulletin A-3600N)



Note: Be sure to check Globe for latest data prior to preparing spec. control prints.

Type GRP precision permanent magnet d.c. motors provide extremely high output, and are designed to meet appropriate MIL specs. Various armature windings can be accommodated, making it possible to meet a wide range of speed and torque characteristics. Wound field designs are available in this frame size for series, split series, shunt, split shunt or universal operation. Please submit application details for an engineering recommendation.

rating:  $\frac{1}{2}$  hp, at 8,000 rpm, continuous duty.  
 voltage: 6 to 115 v.d.c.  
 weight: 2 lbs. 8 oz.  
 armature: Impregnated with fungus resistant varnish. Inertia: 165 gm. cm.<sup>2</sup>  
 protection: Housing is cadmium plated to conform to QQ-P-416 Type 2 for protection against moisture, fungus and salt spray.  
 magnets: Alnico V.  
 bearings: Ball bearings are double-shielded, life-lubricated. Standard lubricant conforms to MIL-G-3278. Special lubricants available for temperature extremes.  
 frame: Pole pieces are die cast into aluminum frame by patented technique.  
 shaft: #420 stainless steel shaft is through-hardened to Rc 45-50, and centerless ground to finish of 5 microinches.  
 end bell: Metal end bell with plastic brush holders is standard. Plastic end bell available for special applications.  
 electrical connection: Two 8" leads are provided.  
 reversibility: Motor reverses when terminal voltage is reversed.  
 mounting: Standard mounting is by means of pilot and tapped holes on front face, or by clamping around motor diameter with non-magnetic clamp.

#### STANDARD PART NUMBERS AND DATA

VOLTAGE (v.d.c.)	SPEED no load (rpm)	TORQUE		CURRENT			STANDARD PART NO.*
		max. rated (oz. in.)	nom. stall (oz. in.)	max. no load (amps)	max. rated load (amps)	nom. stall (amps)	
6	4,700-5,300	8.0	36	2.00	7.0	28.0	166A100-4
12	6,300-7,000	8.0	48	1.34	6.0	30.0	166A100-5
12	4,700-5,300	12.0	44	1.00	5.8	25.0	166A100-6
27	8,500-9,500	10.0	70	0.80	3.4	35.0	166A100-7
27	6,500-7,300	13.0	60	0.62	3.4	22.0	166A100-8
27	5,300-5,900	16.0	52	0.50	3.3	12.0	166A100-9
27	4,200-4,800	16.0	52	0.40	2.7	10.0	166A100-10
50	6,300-7,100	14.0	62	0.32	1.9	11.0	166A100-11
50	4,900-5,500	11.5	50	0.25	1.5	6.0	166A100-12
50	3,900-4,400	15.0	44	0.29	1.2	4.0	166A100-13
115	7,300-8,100	12.0	70	0.16	0.90	7.0	166A100-14
115	5,900-6,500	15.5	60	0.14	0.65	4.5	166A100-15
115	4,700-5,300	16.0	56	0.12	0.70	3.0	166A100-16
115	3,700-4,100	15.0	42	0.09	0.50	1.5	166A100-17
115	3,000-3,400	14.5	44	0.07	0.45	1.3	166A100-18
115	2,400-2,700	14.0	28	0.05	0.35	0.7	166A100-19

KAISER  
SPEED CONTROLLER

System SY1010

# DETECTION SCIENCES INC. DIGINAUTICS DIVISION

7731 COUNTRY CLUB DRIVE • MINNEAPOLIS, MINNESOTA 55427 • PHONE (612) 544-1596

## INSTRUCTIONS FOR INSTALLING DETECTION SCIENCES DIGITAL SPEED CONTROL

1. Disconnect all electrical power from the machine by pulling the main fuses or circuit breakers.
2. Install speed controller on control panel.
3. Install motor drive assembly.
4. Connect power and SCR control lines from two of the grey cables to the motor drive assembly as shown in Figure 3. The power lines are #16 AWG and the control lines are #22 AWG.
5. Connect the armature leads of the motor to Terminals A1 and A2 on the motor drive assembly.
6. Attach magnetic pickup using a bracket such that there is approximately 0.003 inch of clearance to the high points of the sprocket teeth (see Figure 2). Insert phone plug on cable into jack on motor sensor bracket.
7. For 115 VAC phase to phase operation, connect the 115 VAC LINE IN and LINE NEUTRAL as shown in Figure 3.

--CAUTION--

Insure phone plug on cable is inserted into jack on motor sensor bracket. If not connected, motor runaway will result.

8. Reconnect electrical power and engage drive switch. Observe direction of rotation of shaft. If direction is proper, go on to step 9. If backwards, remove electrical power and reverse the two armature leads. Reconnect electrical power and observe direction of shaft rotation.
9. Dress the grey cabling for neatness and for clearance to the sprocket and tie down.



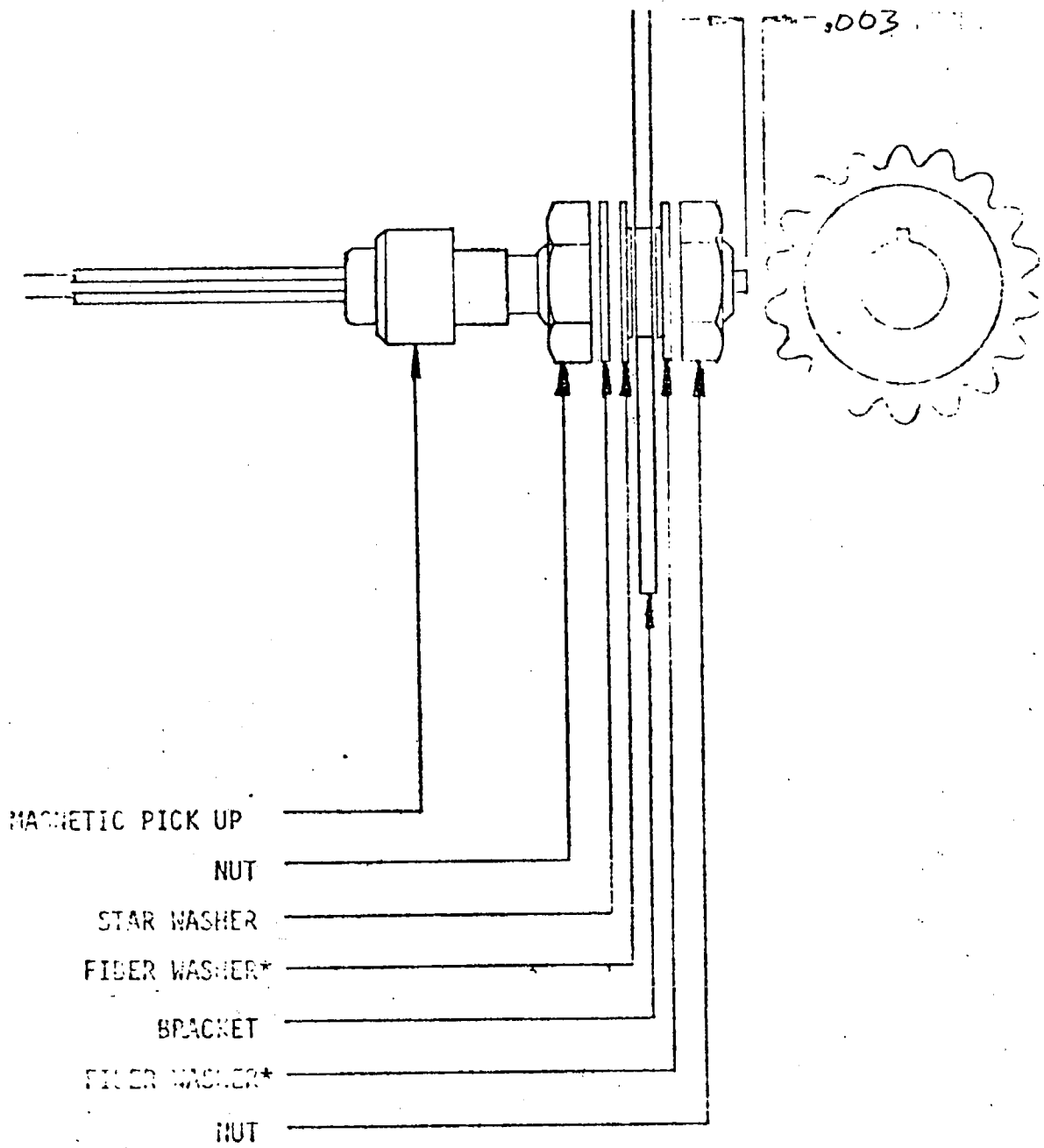
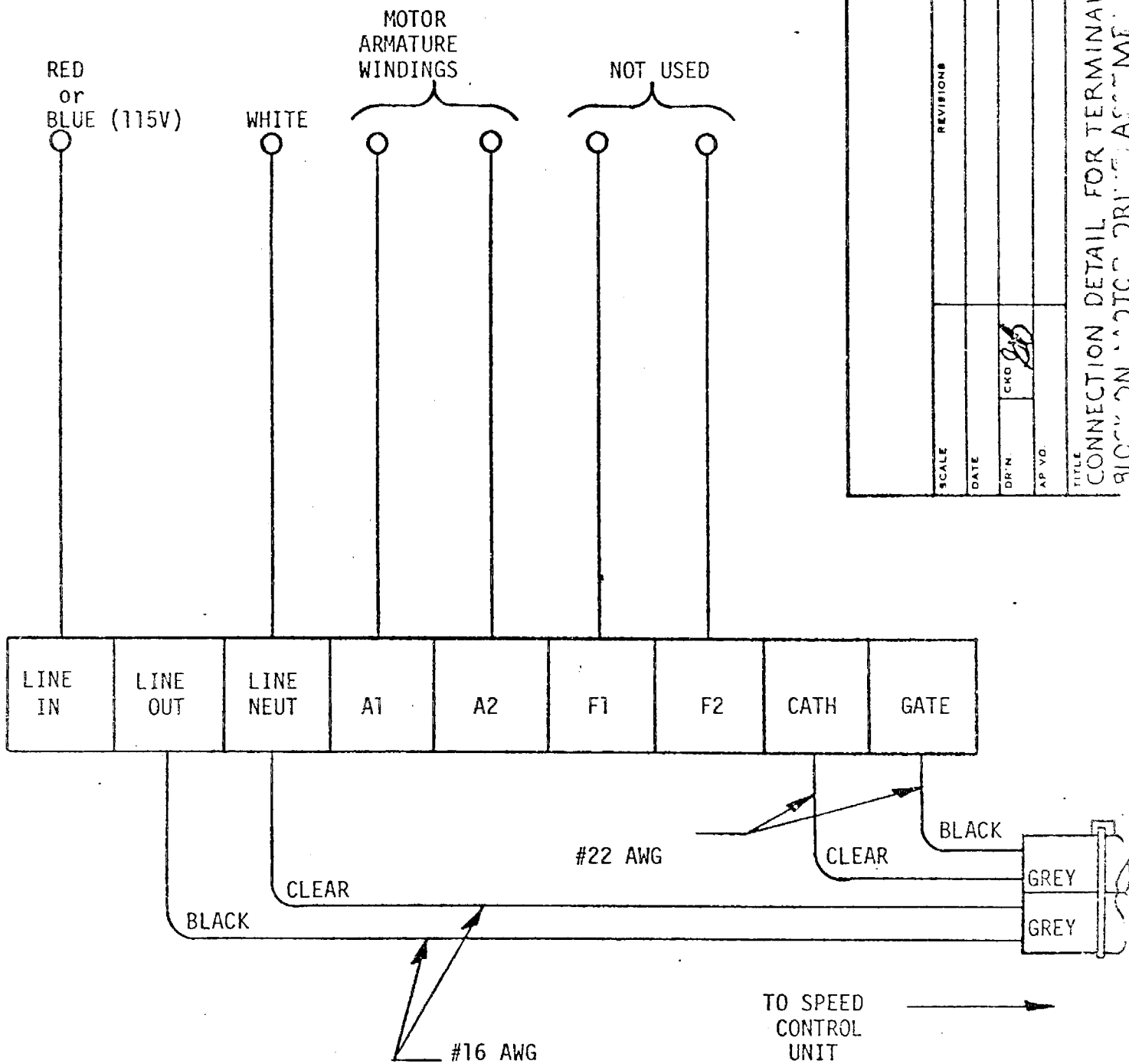


FIGURE 2

ASSY DETAIL OF MAGNETIC PICKUP TO BRACKET

\*NOTE THE DIRECTION OF THE SLOTTED SIDES ON THE FIBER WASHERS. THIS IS TO INSULATE THE PICKUP FROM THE BRACKET.



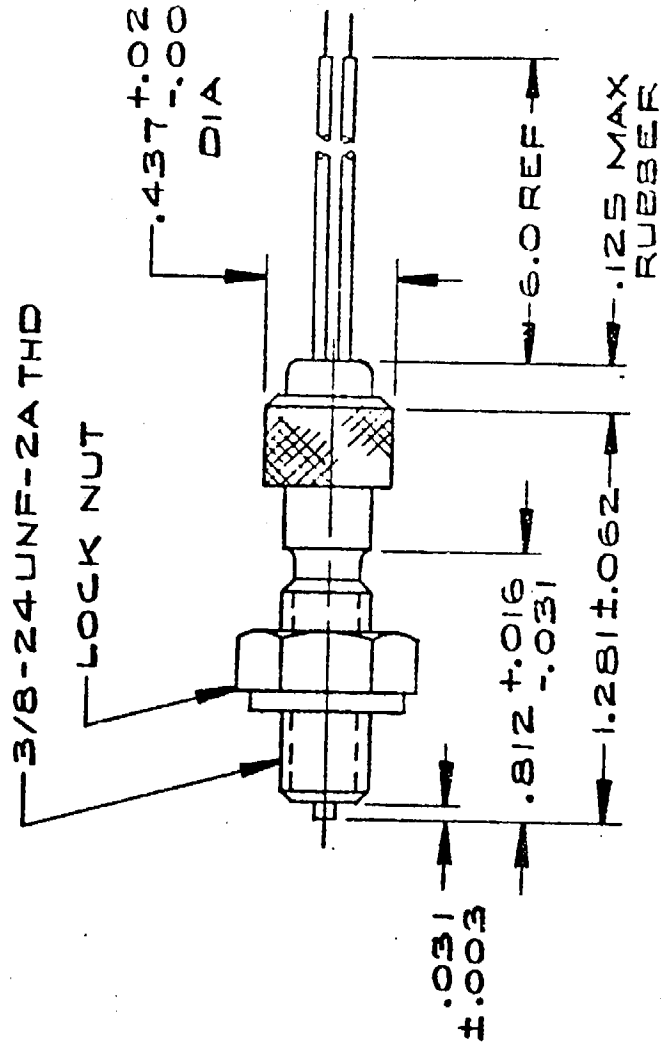
REVISIONS		BY	DATE
SCALE			
DATE			
DRN	CHKD		
AP VO			
TITLE			NO
CONNECTION DETAIL FOR TERMINAL BLOCK ON MOTOR DRIVE ASSEMBLY			MC116-102

FIGURE 3: CONNECTION DETAIL FOR TERMINAL BLOCK ON MOTOR DRIVE ASSEMBLY

CAUTION - IF NOT CONNECTED AS SHOWN, SERIOUS DAMAGE TO THE SPEED CONTROLLER WILL RESULT.

PA T NO.	30179-101	3015-A
REV		
PART NO.		

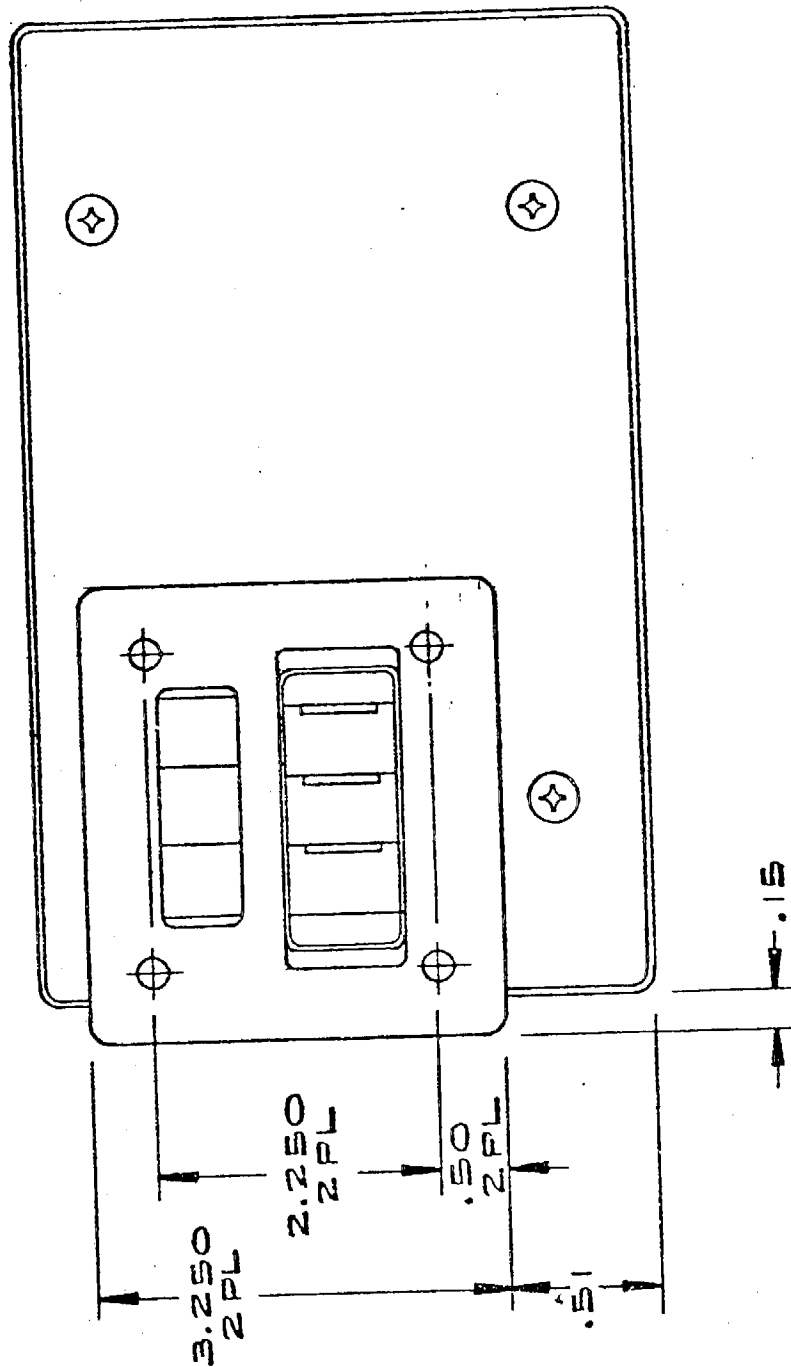
DATE	REV	ECO NO.	REVISION
			DETAIL



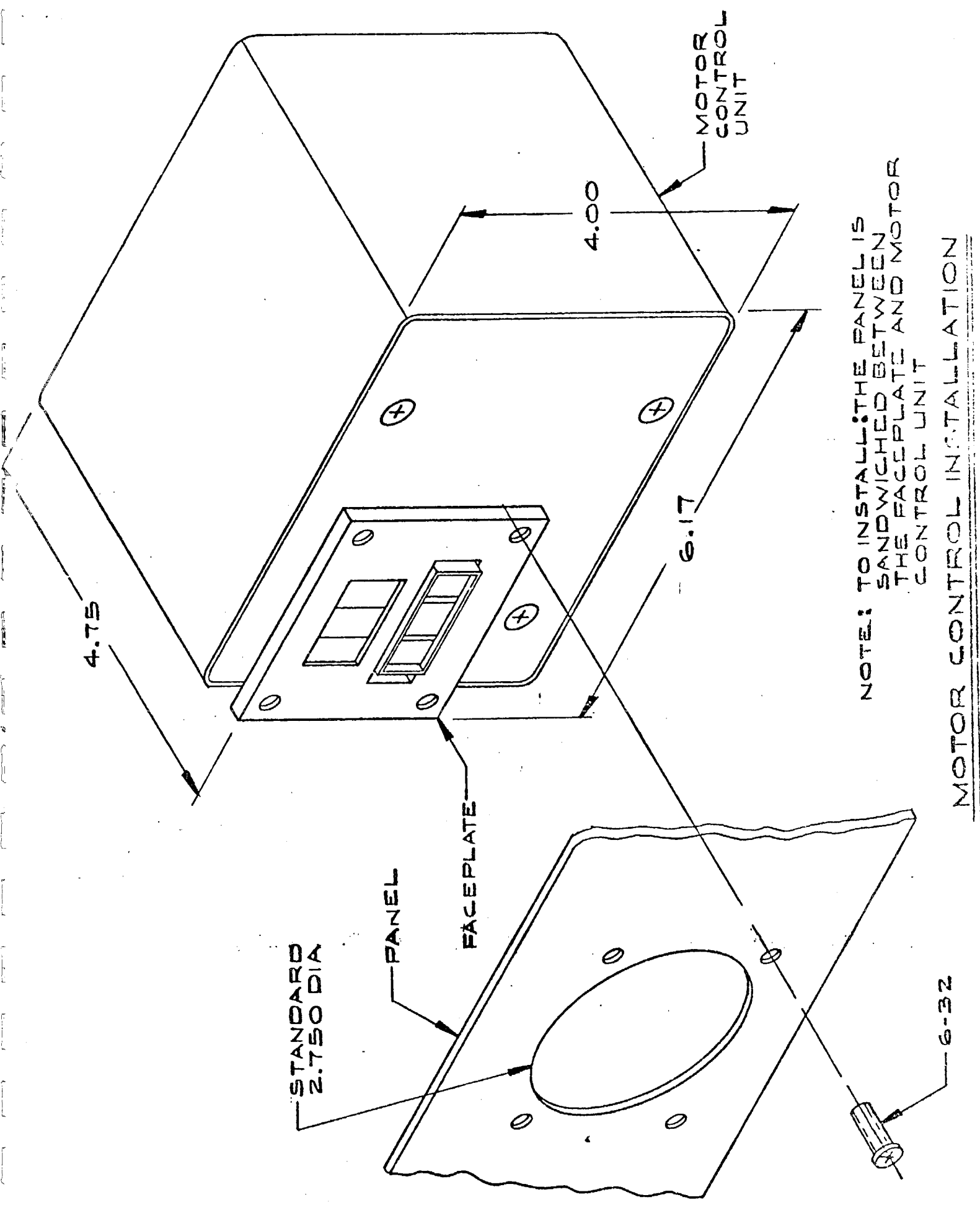
3. INSPECTION REQUIREMENTS:
  - A. ELECT. RESISTANCE TO CASE TO EXCEED ONE MEG OHM.
  - B. DIMENSIONS PER FIG.
2. REQUIREMENTS:
  - A. PEAK TO PEAK TEST VOLTAGE: 15 TO 26, TESTED AT 1,000 IN/SEC WITH 20 PITCH 30 TOOTH GEAR AT 0.005 INCH CLEARANCE AND A LOAD OF 100,000 OHMS.
  - B. RESISTANCE: 90 TO 110 OHMS.
  - C. INDUCTANCE: 22-31 MILLI HENRIES.
  - D. POLARITY: WITH APPROACH OF FERROUS METAL, WHITE LEAD WILL BE POSITIVE WITH RESPECT TO BLACK LEAD.

<b>REVISIONS</b>	
SCALE	NONE
DATE	6-21-72
DRN	AD
CKD	
APVD	L/SELL
TITLE	
BY	
DA	
SENSORE MAGNETIC PICKUP	
NO 30179	

VENDOR(S)	
PRODUCTS LABS	



**MOTOR CONTROL LOCATING  
 DIMENSIONS**



NOTE: TO INSTALL THE PANEL IS SANDWICHED BETWEEN THE FACEPLATE AND MOTOR CONTROL UNIT

MOTOR CONTROL INSTALLATION

## APPENDIX B

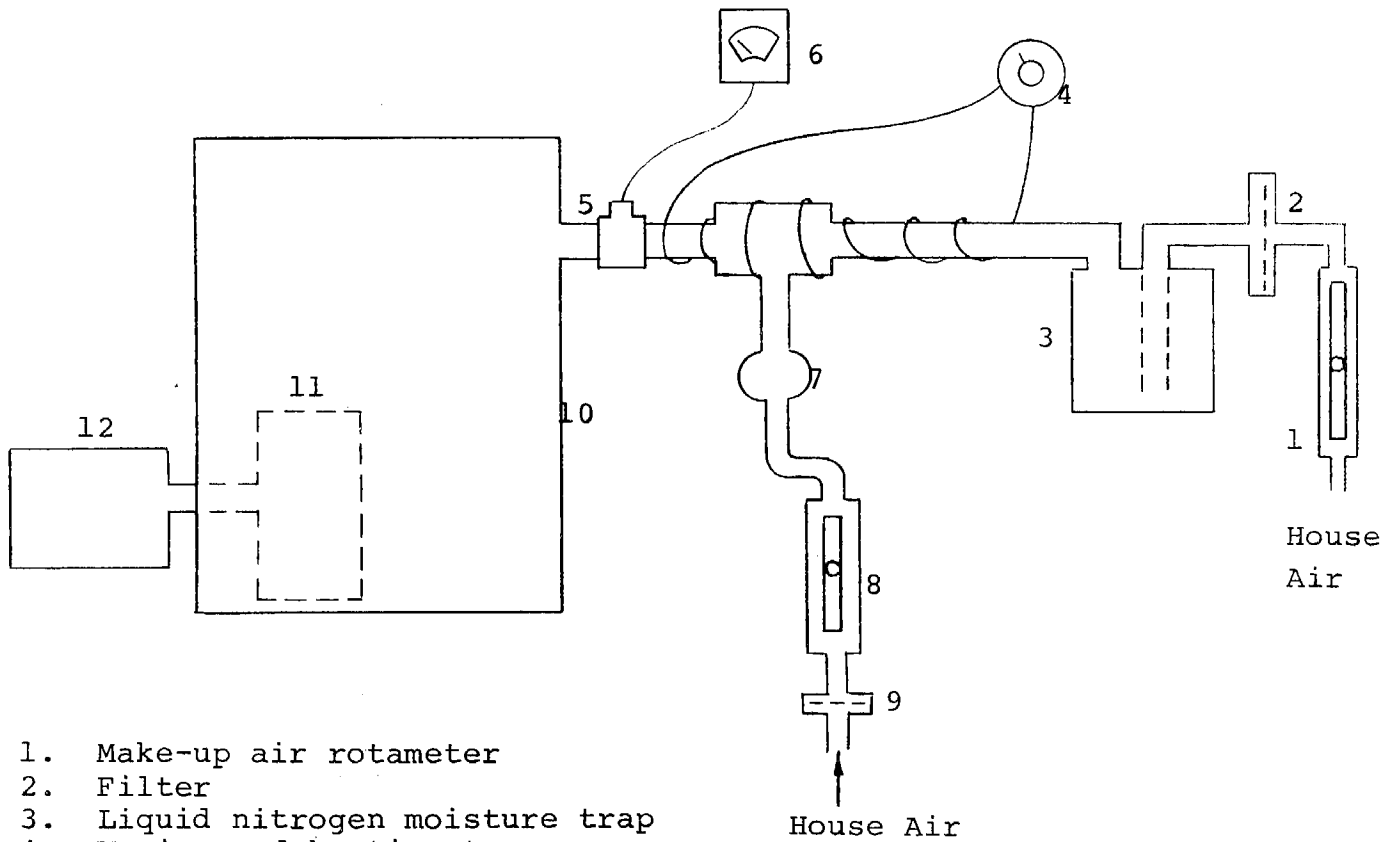
### Aerosol Generator

The aerosol generator used in this study was devised and built at C.F.T. It is a simple arrangement and built inexpensively from readily available components.

A DeVilbiss #42 Aspirator - nebulizer forms a fog from a liquid suspension or solution of the subject aerosol. The aspiration rate is 0.10 to 0.15 ml/min. Inorganic and organic solutions, such as sodium chloride or methylene blue, or suspensions, such as polystyrene latex microspheres, iron oxide "muds", and quartz have all been found amenable to processing. The solution or suspension is made-up in particle free liquid and aspirated with filtered compressed air at about 4-6 l/min. into a glass "T". Filtered and dried make-up air enters a second leg of the "T" at about 5-7 l/min. The make-up air is predried by running it through a liquid nitrogen trap. Heating tape is wrapped around the area of the "T" and the make-up air conductor pipe leading to the T. The combined aerosol stream is heated to about 35°C assuring complete evaporation and the formation of the aerosol. For sampling, the aerosol was conducted to a box in which the sampler was operating.

Such a generator provides considerable latitude in the particulate concentration of the generated aerosol. Varying the concentration of the suspension (solution) and the amount of make-up air can yield particulate concentrations in the practical range of a few hundred to many thousands of micrograms per cubic meter.

The diagram in Figure 34 shows a flow chart of this arrangement.



1. Make-up air rotameter
2. Filter
3. Liquid nitrogen moisture trap
4. Variac and heating tape
5. Therocouple
6. Temperature meter
7. Aspirator-Nebulizer
8. Rotameter
9. Filter
10. Sampling box
11. Centrifuge sampler
12. Sampler motor

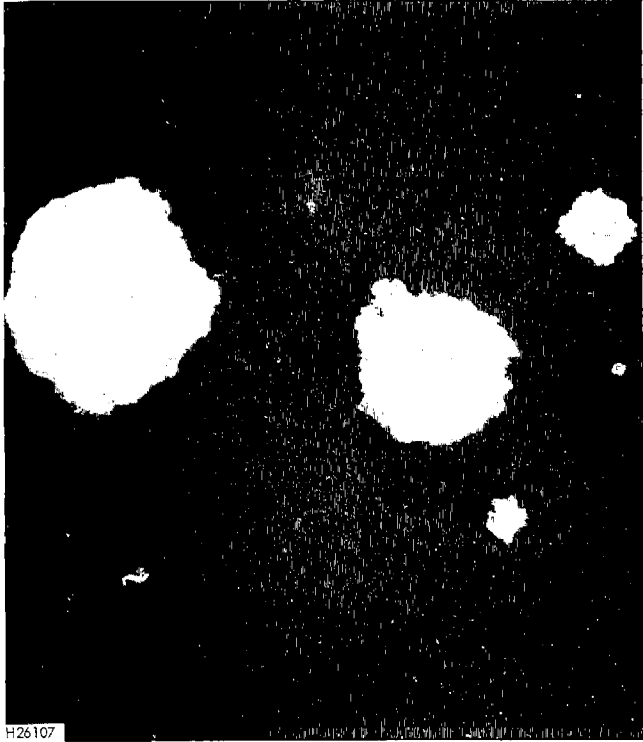
Figure B-1  
FLOW CHART OF THE AEROSOL GENERATOR

## APPENDIX C

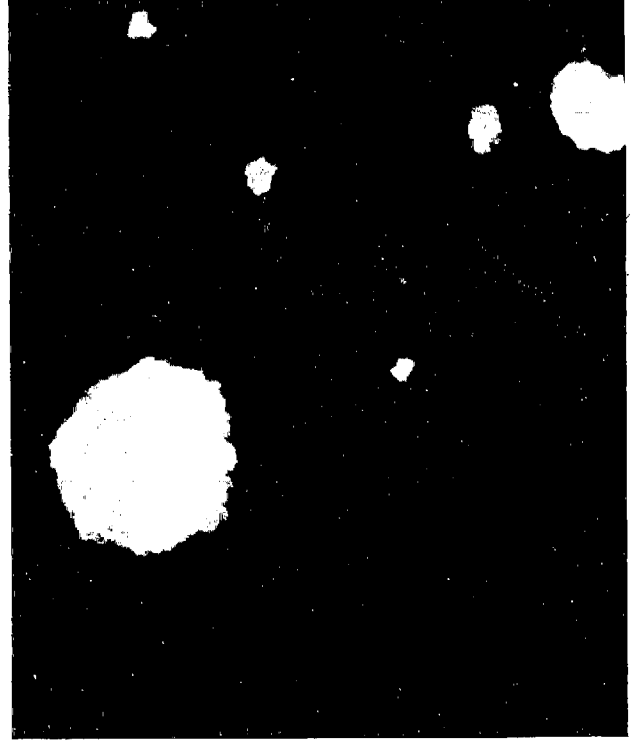
### Description of the Synthetic Aerosol And Its Characterization

The synthetic aerosol used to determine the sampler's entry loss was produced in the aerosol generator described in Appendix B. The precursor of the aerosol was a water suspension of a material which is largely iron oxides. This is a natural by-product of the Bayer process of winning aluminum oxide from bauxite ore. In this process the aluminum oxides of the bauxite are dissolved in a strong caustic soda solution. The insoluble residue mud is mostly iron oxides (hematite and goethite) but also contains mineral oxides of titanium, calcium, etc. and a range of minor and trace elements.

The mud specimen was received as a strongly basic water suspension of approximately 20% solids. The mud was repeatedly washed by dilution and sedimentation to a pH of less than 8 and then brought to a 1% solids concentration. This suspension was usually diluted to 0.5% solids for aspiration and aerosol generation. The particles of the generated aerosol from this material occur predominantly as subspherical aggregates of individual units which are less than 0.1  $\mu\text{m}$  size. The bulk density of the individual aggregates are calculated to be 0.8 to 0.9  $\text{gm}/\text{cm}^3$  by the method described in section 7.2.1. Figure C-1 comprises two photomicrographs of typical particles of the synthetic mud aerosol. These were air sedimented onto SEM sample studs for examination.



10,000X



10,000X

Figure C-1  
TYPICAL AIR SEDIMENTED SYNTHETIC AEROSOL PARTICLES

The first particle size distribution characterization of this synthetic aerosol consisted of air sedimentation and electron microscopic sizing and counting. For this, synthetic aerosol was conducted to a rectangular chamber on which 24 polished aluminum SEM studs had been attached to bottom, top and sides. Aspiration was continued for ten minutes and then allowed eight hours to sediment. Sedimentation time was based on calculated sedimentation velocity for the minimum sized particles of interest. To get the optimum number of particles on the sample studs three aspiration and sedimentation intervals were used.

The samples were then removed and examined by SEM in a pre-selected pattern of fields with twelve fields per stud. The fields were those 2mm in from the edge of the 10mm diameter stud and at 30° rotation intervals. Each field was photographed at 10,000X and 3,000X magnification. The microscope's magnification had been previously calibrated using 0.234  $\mu\text{m}$  and 0.500  $\mu\text{m}$  polystyrene microspheres. The particles contained in the photographed field were measured with a millimeter rule. Particles extending beyond the field of the photomicrograph on the bottom and right hand edges were ignored; particles extending beyond the 10,000X magnification photo on the left edge and top were included by use of the 3,000X photograph. Each particle was measured in two directions, parallel and verticle to the length of the photomicrograph. In all, over 3800 measurements were made. Each of the measurements was placed into an appropriate root-2 size interval. Table C-1 shows a summary of the determined number-size distribution.

TABLE C-I

True Number-Size Distribution Data Summary

<u>Size Interval and Mean Size, <math>\mu\text{m}</math></u>	<u>Individual Number Observed</u>	<u>Individual Number Percent</u>	<u>Cumulative Number</u>	<u>Cumulative Number Percent</u>
0.10 - 0.14 (0.120)	436	11.3	436	11.3
0.15 - 0.19 (0.170)	537	13.9	973	24.3
0.20 - 0.29 (0.245)	614	15.9	1587	41.1
0.30 - 0.40 (0.350)	536	13.9	2123	55.0
0.41 - 0.60 (0.505)	616	16.0	2739	71.0
0.61 - 0.80 (0.705)	388	10.1	3127	81.1
0.81 - 1.13 (0.970)	289	7.5	3416	88.6
1.14 - 1.60 (1.37)	219	5.7	3635	94.3
1.61 - 2.26 (1.93)	136	3.5	3771	97.8
2.27 - 3.20 (2.73)	60	1.6	3831	99.4
3.21 - 4.52 (3.87)	15	0.4	3846	99.8
4.53 - 6.40 (5.47)	9	0.2	3855	100.0
	<u>3855</u>	<u>100.0</u>	<u>3855</u>	<u>100.0</u>

The distribution has a number median diameter of 0.32  $\mu\text{m}$ , a 10-90 number percentile range of 0.1 to 1.0  $\mu\text{m}$ , and a number geometric standard deviation of 2.4.

The second size distribution characterization consisted of sampling an identically generated synthetic aerosol with a five stage Brink cascade inertial impactor. The Brink instrument included a glass cyclone ahead of the collection plates to collect the coarsest fraction and a glass wool filter following the last stage to collect the finest fraction. No weighable amount of particulate was collected in the cyclone; there was significant weight of the finest fraction on the glass wool filter. The mass-size distribution collected was calculated by an available computer program to determine the particle size at 50% capture efficiency. The mass collected on the glass wool filter, of a size less than 0.48  $\mu\text{m}$ , was assumed to be 0.20  $\mu\text{m}$  average for the subsequent calculations.

Using the mean particle size between the upper and lower limits for each interval as the effective size, and 0.20  $\mu\text{m}$  for the material on the filter, the mass distribution was calculated to particle numbers and then to a number distribution. These data are shown in Table C-2.

APPENDIX D

Specific Suppliers

- (1) Beimer Machine Works, Inc.  
7071 Commerce Place  
Pleasanton, Calif. 94566
- (2) VWR Scientific  
San Francisco, Calif.  
Corning Pyrex Brand Cat. No. 237330
- (3) Avnet Electronics  
10916 Washington Blvd.  
Culver City, Calif. 90230
- (4) Detection Sciences, Inc.  
7731 Country Club Drive  
Minneapolis, Minn. 55427
- (5) Electronic Balancing Co.  
2849 Long Beach Blvd.  
Long Beach, Calif.

CARB LIBRARY



07445